Long-term light-curves of transient X-ray pulsars as a tool to study disk−magnetosphere interaction

Master's thesis
University of Turku
Astronomy
June 2022
Sofia Forsblom
Examiners:
Dr. Sergey Tsygankov
Prof. Juri Poutanen

The originality of this thesis has been checked in accordance with the University of Turku quality assurance system using Turnitin Originality Check service.

UNIVERSITY OF TURKU
Department of Physics and Astronomy

Sofia Forsblom Long-term light-curves of transient X-ray pulsars as a tool to study disk−magnetosphere interaction

Master's thesis, 57 pages
Astronomy
June 2022

X-ray pulsars are highly magnetized neutron stars in close binary systems accreting matter from a normal companion star. Their strong magnetic fields channel the accreting matter onto the magnetic poles of the neutron star, releasing an enormous amount of energy in the form of X-rays. If the matter accreted from the stellar companion carries a large amount of angular momentum, it will generally form an accretion disk around the neutron star. The strong magnetic field of the neutron star will effectively truncate the accretion disk at the magnetospheric radius, which defines the space around the X-ray pulsar known as the magnetosphere.

The observed behavior of the X-ray pulsar will depend on several factors, including the rate at which mass is being accreted. At low mass accretion rates, the magnetosphere will be able to extend further out, and if the mass accretion rate drops below some critical value, accreting matter will be stopped by the centrifugal barrier created by the neutron star's rapidly spinning magnetosphere. This is known as the propeller effect, because matter is basically flung out by the rapidly spinning magnetosphere. The propeller effect is generally used to explain the declining phases of the outbursts of transient X-ray pulsars into quiescence.

Another phenomenon recently proposed for transient X-ray pulsars is the possibility of accretion from a cold accretion disk at low mass accretion rates. This is caused by a thermal-viscous instability developing in the accretion disk and is commonly invoked to explain the characteristic outbursts of dwarf novae, where the theory is encapsulated in the disk instability model (DIM). During the decay of dwarf nova outbursts, a propagating cooling front will appear in the accretion disk, and when this front reaches the inner disk radius, the entire disk will be in a cold state of neutral hydrogen.

In this thesis, the data from observations made by the *Swift* observatory have been analyzed with the intent to test the possibility of the appearance of a propagating cooling front during the decaying phases of the outbursts of transient X-ray pulsars. The light-curves of three sources (SMC X-2, 4U 0115+63, V 0332+53) were fitted with a smoothed spline representing the observed behavior, which was subsequently compared to the modeled luminosity decay caused by the propagation of a cooling front. The result of the analysis is that by modeling the expected behavior of a cooling front propagating through the accretion disk, the luminosity decay of these transient X-ray pulsar's outbursts can be well explained without the need to invoke the propeller effect. Additionally, the obtained α_{cold} values are consistent with the values commonly used in the DIM.

Keywords: neutron star, magnetic field, accretion, X-ray binaries

Contents

1 Introduction **1**

2 Accreting X-ray pulsars **3**

2.1 Different kinds of neutron stars 3

2.2 X-ray binaries 5

2.3 The physics of accreting X-ray pulsars 13

2.3.1 Accretion disks 14

2.3.2 Accretion onto a highly magnetized neutron star 19

2.3.3 X-ray spectrum 22

3 Methods **25**

3.1 Overview of the Swift Observatory 25

3.1.1 Swift/BAT 26

3.1.2 Swift/XRT 27

3.2 Data reduction and analysis 29

3.3 Sample of individual sources 31

4 Results and discussion **39**

4.1 Propagating fronts 43

5 Summary and conclusions **49**

References **51**

1 Introduction

Neutron stars are extremely compact objects, possessing extreme physical properties and displaying a broad range of observational phenomena. Emission from different classes of neutron stars spans the entire electromagnetic spectrum, and an equally diverse set of radiative properties.

A **neutron star** is the compact remnant resulting from the explosion of a massive star. Neutron stars are like gigantic nuclei, making them the most dense objects in the Universe. For a typical mass in the range $1.25 - 2.0\mathrm{M}_{\odot}$ and radius in the range $10 - 15$ km, the mean density is $\sim 6.7 \times 10^{14}$ g cm^{-3} (compared to the density of nuclear matter $\sim 2.7 \times 10^{14}$ g cm^{-3}). Neutron stars form unique laboratories, not only for their extreme densities and gravity, but also magnetic fields. The magnetic fields of neutron stars are generally attributed to the conservation of the magnetic flux of the progenitor star, which gives rise to magnetic field strengths as high[1] as $B \sim 10^{13}$ G [2][3].

A large fraction of the known neutron star population are isolated neutron stars, however, some appear in binary systems with companion stars. If the binary system is close enough, they may accrete matter from their stellar companion. The accreted matter is subsequently converted into a huge amount of energy once it hits the surface of the neutron star. If the magnetic field strength of the neutron star is strong enough, it will be able to confine the accreting matter to the magnetic poles of the neutron star, producing hot-spots that are bright in X-rays. As the neutron star rotates, the hot-spots enter the field-of-view of the observer, leading to observations of pulsed X-ray emission. These are known as **accreting X-ray pulsars**, and not only does the strong magnetic field of these pulsars dictate where the energy is dissipated onto the surface of the neutron star, it also dominates how matter is accreted. One simple way to illustrate the strength of the magnetic field of an

[1]Due to the dynamo effect [1], magnetars can be formed with $B \sim 10^{15}$ G.

accreting X-ray pulsar is by the size of its magnetosphere, which co-rotates with the neutron star. During the accretion process, the accreting flow of matter exerts a ram pressure on the magnetosphere, which is counter-balanced by the pressure of the neutron star's magnetic field. Therefore, the extent of the magnetosphere is not only determined by the magnetic field of the neutron star, but also by the rate at which matter is being accreted, i.e. the mass accretion rate. The neutron star's magnetosphere has a significant impact on the accretion process, where the interaction of accreting matter with the magnetosphere determines temporal and spectral characteristics of X-ray pulsars. In turn, a large amount of information about the interaction between the neutron star and the accreting matter can be inferred from observations of these characteristics. If an accretion disk is present in the binary system, conclusions on interactions between the accretion disk and the magnetic field of the neutron star can be made as well. This work attempts to present a new method for studying the physical conditions in the accretion disk and disk-magnetospheric interactions of X-ray pulsars. This is done by investigating the long-term evolution of the luminosity of transiently accreting X-ray pulsars, which reflects changes in the accretion disk's physical properties.

The thesis is organized by the following structure. Chapter 2 gives an introduction to different kinds of neutron stars, X-ray binary systems, and the physics of highly magnetized X-ray pulsars. Chapter 3 describes the *Swift* observatory, including the BAT and XRT instruments used for the observations analyzed in this work. This is followed by the data analysis of the *Swift* observations of each source. This analysis is based on producing the light-curve of each source, which is then fitted with a spline. In Chapter 4, the results of the data analysis are discussed and an interpretation is provided in the context of the disk instability model. In Chapter 5, a summary of the results is given and final conclusions are made.

2 Accreting X-ray pulsars

2.1 Different kinds of neutron stars

The existence of neutron stars was first postulated by Lev Landau in 1932 [4], and later proposed as the remnants of supernovae by Walter Baade and Fritz Zwicky in 1934 [5]. Neutron stars are formed in supernova explosions during the gravitational collapse of massive stars ($M > 8\mathrm{M}_{\odot}$), where the core of the progenitor star is compressed to the point where only neutron degeneracy pressure can prevent further collapse. When the mass of the neutron star exceeds the Tolman-Oppenheimer-Volkoff limit (the maximum mass of a cold, non-rotating neutron star), neutron degeneracy pressure can no longer support the neutron star and it collapses, forming a black hole. During the collapse of the massive progenitor star, the rate of rotation increases due to the conservation of angular momentum. Therefore, newly born neutron stars can rotate several hundred times per second.

A **pulsar** is simply the observational manifestation of a rapidly rotating neutron star emitting beams of radiation, leading to a pulsed appearance of emission when the beam of radiation is displaced from the rotational axis. This is only observable when the beam comes into the observer's field of view, something often described as the "lighthouse effect". Radio pulsars were initially discovered by Jocelyn Bell and Anthony Hewish in 1967 [6], marking the first observational evidence supporting the existence of neutron stars. Most of the known neutron star population are isolated radio pulsars, which are regularly pulsating sources of radio waves, spinning down due to the loss of rotational energy. However, neutron stars are also found in binary systems.

A large fraction of all stars are part of binary systems. The more massive star evolves first and depending on its mass, eventually, it may explode as a supernova with the remnant being a neutron star. If the binary system survives the supernova

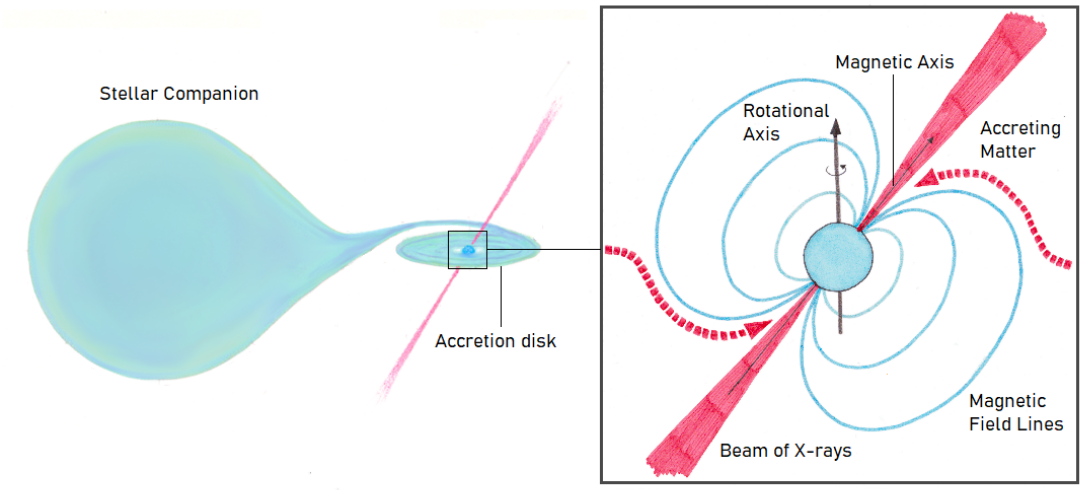

Figure 1. A simplified schematic of an X-ray pulsar, where the accreted matter from the stellar companion provides the source of X-ray emission as it is channeled by the strong magnetic field of the neutron star onto its magnetic poles.

explosion, it will consist of a neutron star gravitationally bound to a stellar companion. In a sufficiently close binary system with a normal star, the neutron star can accrete matter from its stellar companion. The accretion flow is controlled by the strong magnetic field in the vicinity of the neutron star, forcing accreting matter to follow the magnetic field lines onto the magnetic poles [7]. Once the accreted matter falls onto the surface of the neutron star, it produces hot-spots that are bright in X-rays, rotating in and out of the observer's field-of-view giving the appearance of pulsed emission. These are accreting **X-ray pulsars** (see Figure 1), and the accretion of matter transfers angular momentum to the neutron star, causing it to either spin up or spin down, depending on the neutron star's rotation, magnetic field strength, as well as the rate of mass accretion.

Radio pulsars, which are rotation-powered, and X-ray pulsars, which are accretion-powered, display different observational properties and have an important difference in the underlying physics responsible for their characteristic behavior. Rotation-powered pulsars are the "classical" pulsars, most commonly associated with radio

pulsars. They are powered by the loss off rotational energy due to braking by their magnetic fields ($B \sim 10^{8-13}$ G). The intense beam of radiation is a result of the rotation of the strong magnetic field, which causes an electric potential to develop at the magnetic poles of the neutron star which is able to extract particles from the surface [8]. The open magnetic field lines at the magnetic poles of the neutron star act as escape valves for the charged particles, producing beams of radio emission. Magnetars represent a separate, extreme breed of isolated, slowly rotating neutron stars that are characterized by variable X-ray activity powered by the dissipation of immense magnetic fields ($B \sim 10^{13-15}$ G). An overview of different examples of isolated and non-accreting neutron stars can be found in, e.g. [9][10].

Accretion-powered pulsars (or accreting X-ray pulsars) are, as the name suggests, powered by accretion, where the gravitational potential energy of matter accreted from a close companion star powers the X-ray emission. In contrast to rotation-powered pulsars, accreting X-ray pulsars can display large temporal variability in both the spin period of the neutron star and the observed luminosity of the source. Some accreting X-ray pulsars are persistent sources, while others are transient sources that are only observable during shorter episodes of intense activity in X-ray emission, but mostly remain in quiescence. X-ray pulsars also have some of the strongest magnetic fields in the entire Universe, as high as several 10^{12} G. Such strong magnetic fields are essential for the production of the pulsed X-ray emission of X-ray pulsars, as it channels the accreting matter onto the magnetic poles of the neutron star, instead of allowing it to reach the entire surface.

2.2 X-ray binaries

Accreting X-ray pulsars are part of so-called **X-ray binaries** (XRBs). X-ray binaries can simply be defined as systems consisting of a compact object in a close

binary system with a normal stellar companion[2]. By close binary system, it means that there is a transfer of mass between the stellar companion and the compact object, which is essential for powering the X-ray emission. Pulsed X-ray emission from a binary system were first discovered by Giacconi et al. [11] in the early 1970's during observations of Centaurus X-3 with the *UHURU* observatory, and analysis by Schreier et al. [12] subsequently revealed the source's binary nature. Shortly after this, Tananbaum et al. [13] discovered another X-ray pulsar, Hercules X-1, displaying similar characteristics.

Accreting X-ray binaries are among the brightest X-ray sources in our Galaxy. The X-ray emission of these binaries is powered by the dissipation of gravitational potential energy in the matter accreted from the stellar companion onto the compact object, which can be either a white dwarf, neutron star or black hole. X-ray binaries can be divided into two groups based on the mass of the stellar companion: **high-mass X-ray binaries** (hereafter HMXBs), and **low-mass X-ray binaries** (hereafter LMXBs). It is worth noting that there exists a handful of binary systems where the stellar companion is of intermediate mass, often referred to as intermediate X-ray binaries (IMXBs).

The spectral type of the stellar companion, which is also frequently called the donor star or mass donor, determines the mode of transferring mass to the compact object and the surrounding environment [14]. HMXBs conventionally have young stellar companions of spectral type OB and masses $\geq 10\mathrm{M}_{\odot}$, while LMXBs have older stellar companions (spectral type later than A), with masses in general $\leq 1\mathrm{M}_{\odot}$. HMXBs and LMXBs display distinctly different Galactic distributions. HMXBs are concentrated along the Galactic plane, close to their place of birth. LMXBs, on the other hand, populate the Galactic bulge and globular clusters, where they can form through the process of stellar capture [15].

[2]Sometimes referred to as the optical companion, which points to the fact that nuclear burning is still taking place in its interior.

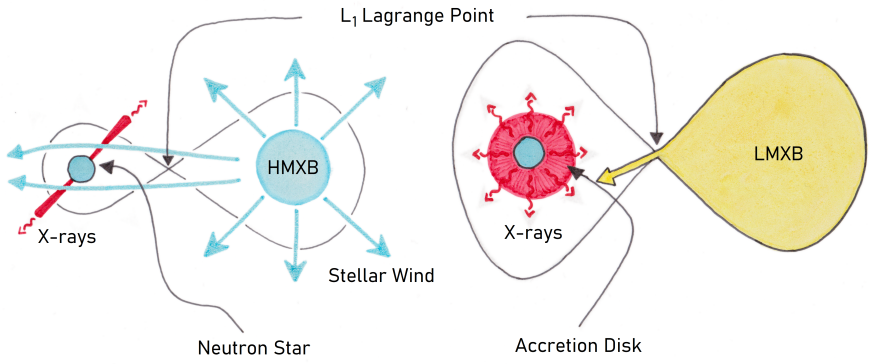

Figure 2. Simplified view of the general difference between accretion in HMXBs and LMXBs. For the HXMB, a $M \geq 10\mathrm{M}_{\odot}$ stellar companion of a $M \sim 1.4\mathrm{M}_{\odot}$ neutron star provides matter through its stellar wind, while for the LMXB, a $M \leq 1\mathrm{M}_{\odot}$ companion star overflows its Roche lobe, allowing matter to be captured and accreted by the neutron star through the formation of an accretion disk.

Accretion of matter is generally different for LMXBs and HMXBs, taking place through either **Roche-lobe overflow** or **wind accretion** (see Figure 2). Typically for LMXBs, Roche-lobe overflow occurs as the small and low-mass donor star evolves, causing its Roche lobe[3] to fill up and overflow. Matter outside of the donor star's Roche lobe is no longer bound by gravity and can therefore be accreted by the compact object [16]. Because the accreting matter carries a significant amount of specific angular momentum, it tends to form an accretion disk around the compact object, as opposed to being directly accreted (see Section 2.3.1). In the case of HMXBs, accretion can occur through Roche-lobe overflow, however, this is generally not the case. Instead, wind accretion largely takes place in HMXBs. The OB stellar companions of HMXBs have very slow but dense stellar winds. The compact object typically orbits the stellar companion at a close distance, and is therefore heavily embedded in the stellar wind. The accreted wind carries a comparably small amount of angular momentum relative to the compact object, and therefore wind-fed systems

[3]The Roche lobe defines the region around a star in a binary system in which material is bound to that star by gravity.

generally accrete directly in a quasi-spherical manner without the formation of an accretion disk. A hybrid situation is often observed in neutron star X-ray binaries with very eccentric orbits (known as Be/X-ray binaries), where an accretion disk may temporarily form due to a significant increase in mass accretion during periastron passage.

In the case of **neutron star X-ray binaries**, the compact object is a neutron star and a strong X-ray emitter. The magnetic field of the neutron star plays an important role in determining where the energy of accreting matter is dissipated. High surface magnetic fields ($B \sim 10^{11-14}$ G) are generally observed for neutron stars in young HMXBs, while lower surface magnetic fields ($B \lesssim 10^{10}$ G) are present in the much older LMXBs, where the magnetic field has decayed over time. When the magnetic field of the neutron star is greater than $\sim 10^8$ G, it is strong enough to channel the accreting flow onto restricted regions close to the magnetic poles. This results in X-ray pulsations at the spin period of the neutron star when its magnetic axis is displaced from its rotational axis. Considering the high magnetic fields that tend to be found for neutron stars existing in HMXBs, they generally appear as X-ray pulsars. When the magnetic field is below $\sim 10^8$ G, the accreting flow is able to reach all the way down to the surface of the neutron star before it is captured by the magnetic field. In low magnetized systems, accreted matter is allowed to accumulate onto the surface of the neutron star, which allows for the ignition of powerful, explosive thermonuclear burning, resulting in so-called Type I X-ray bursts. Therefore, many LMXBs are observed as X-ray bursters, though there are a few systems where the neutron star is capable of producing X-ray pulsations.

An important subclass of LMXBs are **accreting millisecond pulsars** (AMPs) that, according to the "recycling scenario", form an important link to millisecond radio pulsars (MSPs) [17]. The recycling scenario offers an explanation to the fast ms-rotation of old MSPs in terms of the "recycling" of these neutron stars in LMXBs

[18]. AMPs have fast spin periods but relatively low magnetic fields ($\sim 10^8$ G) that have decayed by higher than typical values. It has been suggested that they are, in fact, old neutron stars that have been recycled and spun-up during a Gyr-long phase of mass accretion transferred through the accretion disk of a low-mass stellar companion [19][20][21]. Once the accretion ceases, a rotation-powered pulsar turns on, emitting most of its radiation in the radio band.

Neutron star HMXBs can be subdivided into two groups depending on the evolutionary status of the stellar companion: those with main-sequence Be stellar companions, **Be/X-ray binaries** (hereafter BeXBs), and those with evolved OB supergiant companions, **supergiant X-ray binaries** (hereafter SGXBs). Accretion in HMXBs can occur in different ways, and observationally one distinguishes between disk-fed SGXBs, wind-fed SGXBs, and the aforementioned BeXBs, where accretion occurs due to the interaction between the neutron star and the decretion disk[4] around the Be stellar companion [22].

Supergiant X-ray binaries

In the majority of all SGXBs, the neutron star directly captures a small fraction of the stellar wind of its companion star [23][24] and the resulting accretion rates generally remain low. Therefore, their X-ray luminosities tend to be lower as well. These moderate-luminosity, **wind-fed SGXBs** concern close systems ($P_{orb} < 15$ d) with low eccentricities. In wind-fed SGXBs, the donor star emits a steady and substantial stellar wind, removing between $10^{-6} - 10^{-8}$ $M_\odot$/yr, therefore, a neutron star in a relatively close orbit will capture some fraction of this wind [14]. Even though wind accretion is an ineffective process, it can make for a sizeable mass accretion rate onto the surface of the neutron star, thanks to the high mass-loss rate of the stellar companion, resulting in a bright X-ray source.

[4]The rapid rotation of Be stars causes material to be ejected from their surfaces, leading to a diffuse and gaseous circumstellar disk, commonly referred to as a decretion disk.

If the donor star is beginning Roche-lobe overflow, material with high specific angular momentum will start to flow through the L_1 Lagrangian point[5], leading to the development of an enhanced stream of wind known as a tidal stream. This funnels the wind through the tidal stream and increases the wind density close to the neutron star, consequently increasing the X-ray luminosity [25]. If the specific angular momentum of the wind is large enough, an accretion disk may form around the neutron star. This type of accretion is very efficient and results in a mass transfer rate significantly greater than what is possible by the neutron star just capturing some fraction of the stellar wind of the companion star [7]. When mass transfer takes place via Roche-lobe overflow, the X-ray emission is highly enhanced and these **disk-fed SGXBs** tend to become very luminous (up to 10^{40} erg/s) [26]. However, it is uncommon to observe Roche-lobe overflow in HMXBs, because the neutron star is quickly submerged in the atmosphere of its stellar companion because of the large mass ratio [27], resulting in something known as the "common envelope phase" [28].

Be/X-ray binaries

BeXBs account for a substantial part of all HMXBs and virtually all systems show X-ray pulsations. The Be stellar companions are rapidly rotating B-type stars that have displayed spectral emission lines at some point during their lifetime, hence the use of the identifier “e” in their spectral types [29][30]. In BeXBs, the compact object is a neutron star in a wide and eccentric orbit, spending a short amount of time close to the dense circumstellar disk that surrounds the fast-rotating Be stellar companion (i.e., the **decretion disk**). Strong and transient X-ray outbursts are expected when the neutron star interacts with this decretion disk, accreting from the low-velocity and high-density wind [31] (see figure 3 for a schematic over a BeXB).

[5]The L_1 Lagrangian point, or inner Lagrange point, acts as a "funnel" between the two objects, where matter can flow freely from one object to the other.

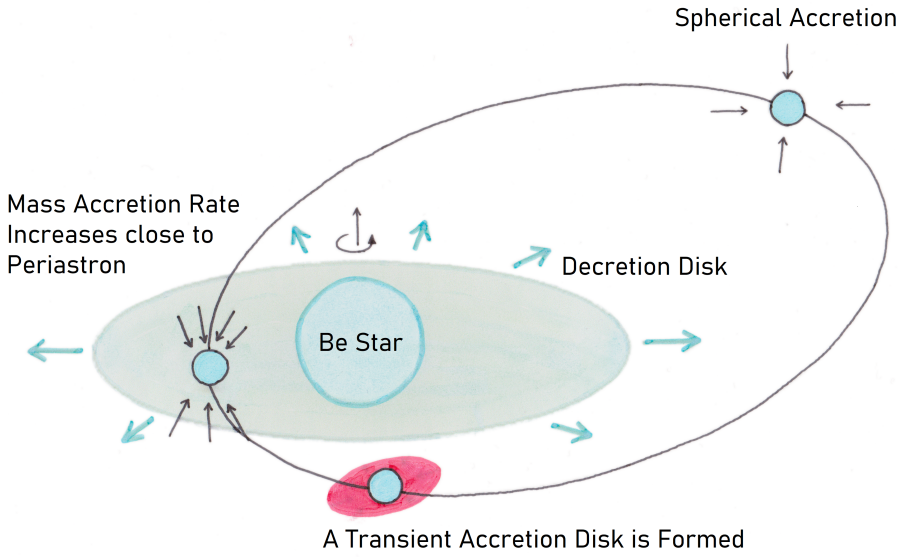

Figure 3. A schematic picture of a BeXB, consisting of a neutron star in an eccentric orbit around a Be stellar companion, periodically passing through its decretion disk.

These X-ray outbursts are often connected to the time of periastron passage of the neutron star in its orbit, when the two objects are at their closest approach. The neutron star will move close-by the decretion disk during periastron (and may even go through it), which causes major disruption [14]. This results in a large amount of matter being accreted onto the neutron star. Two types of outbursts are observed in BeXBs. Normal, **Type I outbursts** appear periodically as a result of an increase in the mass accretion rate close to periastron. They last for $0.2 - 0.3\,P_{orb}$ and peak to luminosities $\leq 10^{37}$ erg s^{-1} [15]. The rare, giant **Type II outbursts** are much larger than Type I outbursts, occurring generally once in several years. Type II outbursts reach peak luminosities exceeding 10^{37-38} erg s^{-1} and last for several orbital periods. Type II outbursts are not linked to the orbital period of the system, instead they tend to be preceded by increased activity of the Be stellar companion. This can affect several characteristics of the decretion disk, therefore influencing the X-ray emission as the neutron star interacts with the material of the disk.

Some BeXBs seem permanently active (persistent systems), while the majority are transient systems, suddenly entering the Be phase for longer periods of time. Persistent BeXBs are different than transient BeXBs in that they display much less X-ray variability (i.e., larger outbursts are not observed), lower luminosities ($L_X \leq 10^{35}$ erg/s), they contain slowly rotating neutron stars ($P_{spin} > 200$ s) and are found in systems with wider orbits ($P_{orb} > 200$ d) [14]. BeXBs are defined as non-supergiant systems and have large orbital periods. Because of this, the Be star is well within its Roche lobe, however, in some instances transient Roche-lobe overflow can take place, e.g., during periastron passage for BeXBs with large and eccentric orbits or during Type II outbursts [14]. The accreted matter is funneled through the L_1 Lagrangian point with high specific angular momentum and therefore tends to form a transient accretion disk around the neutron star. For a review on BeXBs, see e.g. [14].

The transient nature of BeXB systems make them ideally suited for testing different theoretical predictions of accretion physics over a range of regimes not possible in persistent sources. BeXBs are unique systems, as they exhibit substantial transient activity, allowing for the study of interactions between accreting matter and the magnetosphere over a large range in luminosities during outbursts, related to variations in mass accretion rates that can cover several orders of magnitude. They can be utilized to investigate the properties of matter under extreme conditions of magnetic fields, which tend to be quite accurately known thanks to the detection of cyclotron lines in their X-ray spectra. In addition to this, they allow for the possibility of studying accretion disks unaffected by the continuous flow of accreting matter, as an accretion disk is formed during periastron passage, but is "cut-off" from the accretion flow supplied by the companion star's decretion disk as the neutron star continues in its eccentric orbit.

2.3 The physics of accreting X-ray pulsars

X-ray binaries are simply powered by a compact object capturing some of the matter that their close stellar companion "throws out". When matter is accreted onto a compact object, it releases enormous amounts of gravitational potential energy, resulting in the emission of predominantly X-rays. Accretion is a very efficient method of producing energy; the gravitational potential energy released for a compact object of mass M_* and radius R_* when a mass M is accreted is given by:

$$E_{acc} = G\frac{M_* M}{R_*} = \left(\frac{R_S}{2R_*}\right) Mc^2, \tag{1}$$

where G is the gravitational constant, c is the speed of light, and $R_S = 2GM_*/c^2$ is the Schwarzschild radius. When the compact object is a neutron star ($M_* \sim 1.4\mathrm{M}_\odot$, $R_* \sim 10^6$ cm) the energy released is about 20% of the rest-mass energy of the accreted matter. This can be compared to nuclear fusion of hydrogen into helium, which yields $E_{nuc} \sim 0.007mc^2$; therefore accretion onto a compact object is an even more efficient energy source. For a fixed value of M_*/R_*, the resulting **accretion luminosity** depends on the mass accretion rate $\dot{M}$:

$$L_{acc} = \frac{dE_{acc}}{dt} = \frac{GM_*}{R_*}\frac{dM}{dt} = \frac{GM_*\dot{M}}{R_*}. \tag{2}$$

In theory, an upper limit to the accretion luminosity is given by the **Eddington luminosity**, L_{Edd}, at which the outward force produced by the pressure of radiation equals the inward gravitational force. For steady, spherically symmetrical accretion of material mainly consisting of fully ionized hydrogen:

$$L_{Edd} = \frac{4\pi GM_* m_p c}{\sigma_T} \simeq 1.3 \times 10^{38}\left(\frac{M_*}{M_\odot}\right) \ \ [\mathrm{erg/s}], \tag{3}$$

where m_p is the proton mass and σ_T is the Thomson cross-section.

The typical luminosities observed in bright X-ray binaries are of the order of $\sim 10^{36-38}$ erg/s, corresponding to mass accretion rates of $\sim 10^{16-18}$ g/s. Much lower luminosities (down to $\sim 10^{31}$ erg/s) are seen in transient sources during quiescence,

however, it is important to note that this is not necessarily due to accretion, but more likely residual thermal emission instead. [32]

2.3.1 Accretion disks

A compact object in a static, uniform gaseous medium will accrete matter from the environment surrounding it, something referred to as spherical accretion [33]. However, spherical accretion only applies when the specific angular momentum of the gas is negligible. Many accretion flows related to astrophysics are rotating rapidly, and an important question is how to get rid of angular momentum, allowing for matter to be accreted. While viscous dissipation can convert energy into heat (which is subsequently radiated away), angular momentum turns out to be more challenging to remove. When the accreting gas possesses high specific angular momentum, it generally forms an **accretion disk**.

Accretion disks can be described as rotationally flattened structures consisting of gaseous matter spiraling onto a central self-gravitating body, which can be a compact object such as a neutron star. The angular velocity Ω of a particle in a circular orbit at a distance r from a point mass M_* in Newtonian gravity is given by:

$$\Omega = \sqrt{\frac{GM_*}{r^3}} = \Omega_K, \tag{4}$$

where G is the gravitational constant and the subscript K denotes Keplerian orbits [34]. The specific angular momentum, given by $h_K = r^2\Omega_K = \sqrt{GM_*r}$, is defined as the angular momentum per unit mass. Because an accretion disk is formed, the considerable amount of specific angular momentum possessed by the accreting matter can be removed, so that matter can be accreted by the central gravitating object. In an accretion disk, the high angular momentum of rotating matter is gradually transported outwards by the turbulent viscosity between adjacent rings of gas. The material of the faster inner layer loses angular momentum and slowly moves towards

the central object, while the adjacent, slower outer layer gains angular momentum, which is subsequently given to the next layer, and so on [35]. This results in a continuous mass flow towards the central object as angular momentum gradually gets transported outwards, which allows for matter to be accreted. As the gaseous matter falls deeper into the potential well of the central object, it releases energy, which is converted into heat. A fraction of this heat is converted into radiation (making the disk luminous), escaping in part and cooling down the disk [36].

The nature of the transport of angular momentum is usually attributed to so-called magneto-hydrodynamical (MHD) turbulence driven by the magnetorotational instability (MRI) [37], which is a fluid instability that causes an accretion disk orbiting a massive central object to become turbulent. The MRI develops when matter in the accretion disk rotates non-rigidly in a weak magnetic field [36]. Generally, a small-scale MHD description is not directly applied for the turbulence, but it is instead described by a phenomenological "alpha-viscosity prescription", which was introduced by Shakura and Sunyaev in 1973 [38] as a parameterization for the turbulent viscosity. The model introduced by Shakura and Sunyaev, known as the **standard accretion disk model** or ***α*-disk model**, described a relatively cold accretion disk, that was also assumed to be geometrically thin and optically thick [35]. The geometrical thickness of an accretion disk H at radial coordinate r is expected to be much smaller than r:

$$\frac{H}{r} \ll 1. \tag{5}$$

The disk scale height, determined by the local temperature, can be estimated as $H \equiv c_s/\Omega_K$, where the sound speed in the accretion disk, c_s, for a geometrically thin disk, by definition, is much smaller than the Keplerian orbital velocity.

The physics of accretion disks is often described in terms of dynamical, thermal and viscous processes that take place on different characteristic time-scales [34][36]. These are the typical time-scales on which the disk structure may vary. The short-

est characteristic time-scale is the dynamical time-scale (the time-scale of orbital motion), which for a Keplerian disk is given by:

$$t_{dyn} = \Omega_K^{-1}. \tag{6}$$

The viscous time-scale is the time-scale of radial motion in the disk. The viscous time-scale is also the time-scale of surface density evolution, if the surface density is not in steady-state [34]. The viscous time-scale gives the time-scale on which matter diffuses through the disk over a radial distance r, under the effect of viscous torques, and is given by:

$$t_{visc} \approx \frac{r^2}{\nu}, \tag{7}$$

where ν is the kinematic turbulent viscosity. One can insert the α-prescription into Equation 7 (which is typically given by the form $\nu = \alpha c_s H$), together with $H \equiv c_s/\Omega_K$, obtaining:

$$t_{visc} \sim \frac{1}{\alpha \Omega_K} \left(\frac{H}{r}\right)^{-2}, \tag{8}$$

where $\alpha < 1$ is the dimensionless viscosity parameter. The thermal time-scale can be defined as the time-scale on which the accretion disk would cool, in the case that heating processes were instantly turned off [34]:

$$t_{th} \sim \frac{1}{\alpha \Omega_K}. \tag{9}$$

The thermal time-scale is the shortest time-scale on which the emission from an annulus of the accretion disk is expected to change [34]. The time-scale hierarchy for a thin disk with $\alpha < 1$ is:

$$t_{dyn} < t_{th} \ll t_{visc}. \tag{10}$$

Standard accretion disks are known to be subject to the thermal-viscous instability as a result of partial ionization of hydrogen [36]. Because of this instability, the accretion disk transitions between two states: a hot state of mostly ionized hydrogen and a cold state of neutral hydrogen. This instability is commonly invoked to explain

dwarf nova[6] outbursts. These outbursts are caused by an instability developing in the accretion disk when the central temperature is of the order of the hydrogen ionization temperature and the opacities are strongly dependent on temperature [39]. The ionization state therefore determines the opacity of the accretion disk, which affects the cooling rate in the disk, local temperature and by extension the local geometrical thickness. The geometrical thickness therefore influences the viscosity and mass accretion rate. The dependence of the opacity on temperature sets off a thermal-viscous instability that causes the accretion disk to cycle between the two states. In the quiescent cold state, the disk has an effective temperature < 3000 K, hydrogen is mostly neutral and the mass accretion rate, $\dot{M}$, is less than the mass transfer rate from the stellar companion [40]. Because of the low mass accretion rate (hence low viscosity) matter is accumulated in the accretion disk. In the eruptive hot state, the disk has a high internal temperature $> 10^4$ K, hydrogen is highly ionized and $\dot{M}$ is higher than the mass transfer rate from the stellar companion [40]. This instead allows for accumulated matter to be accreted rapidly. The most widely used model to describe the outbursts of dwarf novae is the thermal-viscous **disk instability model** (DIM) (see, e.g., [41]). The DIM uses the α-disk framework, where the accretion disk is assumed to be geometrically thin, and, importantly, that its angular momentum is always Keplerian [41], which is a good approximation in the case of gas pressure dominated accretion disks. The DIM is often illustrated by plotting the effective temperature, T_{eff}, (or the local mass accretion rate) as a function of the local surface density, Σ. This results in the so-called **S-curve**, which represents local disk equilibria and shows three distinct branches: a cool branch on which hydrogen is largely recombined, a hot branch where hydrogen is fully ionized, and an intermediate branch (see Figure 4) [39].

The hot and cold branches are both found to be stable, however, the intermediate

[6]Dwarf novae are a class of cataclysmic variables (binary systems composed of a white dwarf accreting from a Roche-lobe filling low-mass stellar companion) that undergo regular outbursts.

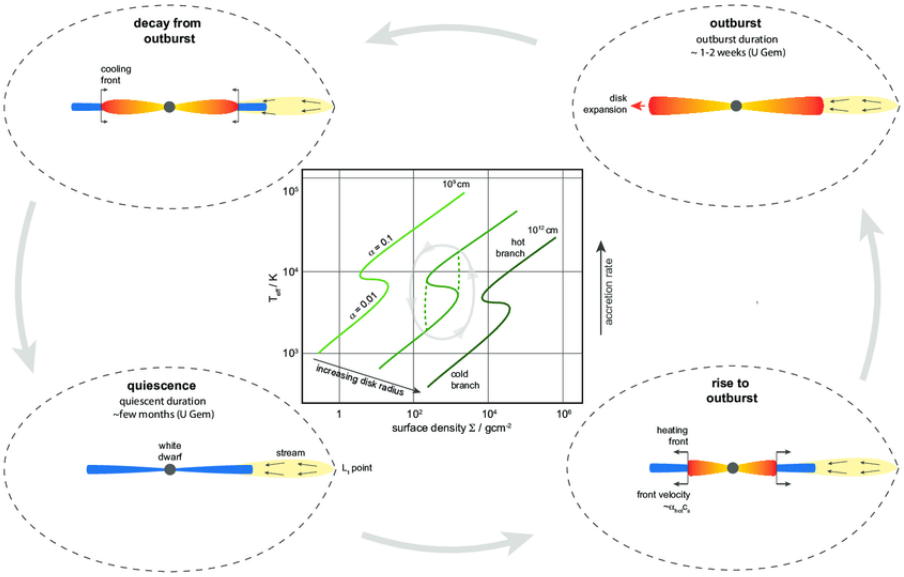

Figure 4. Schematic illustration of how the existence of a local S-curve leads to global outbursts in dwarf novae accretion disks. The S-curves are shown for different radii in the $\Sigma - T_{eff}$ plane for a $1.35 M_{\odot}$ white dwarf. From Armitage [34].

branch is thermally and viscously unstable. The upper transition corresponds to a local mass accretion rate of $\dot{M}^{+}_{crit}$, while the lower transition corresponds to $\dot{M}^{-}_{crit}$, therefore, for local mass accretion rates in the range $\dot{M}^{-}_{crit} < \dot{M} < \dot{M}^{+}_{crit}$ the accretion disk is found to be locally unstable (it is worth noting that both $\dot{M}^{-}_{crit}$ and $\dot{M}^{+}_{crit}$ are independent of α; this is because the temperatures at the transitions are determined by the ionization state of hydrogen). [39]

Until recently, the DIM had not been considered for accreting X-ray pulsars. However, it has been proposed that an X-ray pulsar with a slow enough spin period, combined with a certain magnetic field strength, would transition into a regime of stable accretion from a entirely recombined, cold accretion disk [42]. The effective temperature defining the two different ionization states is the hydrogen ionization temperature ($\sim$ 6500 K), and for a low mass accretion rate the accretion process becomes stable when the temperature of the entire accretion disk falls below this temperature; this corresponds to:

$$\dot{M} < \dot{M}^{-}_{crit} = 3.5 \times 10^{15} r_{10}^{2.65} M_{1.4}^{-0.88} \ \ [\mathrm{g/s}], \tag{11}$$

where $r_{10} = r/10^{10}$ cm is the inner disk radius and $M_{1.4}$ is the mass of the neutron star in units of $1.4M_{\odot}$ [42][43]. Another possible scenario for transient X-ray pulsars accreting at low mass accretion rates is that they end up transitioning into the propeller regime, where matter is stopped by the centrifugal barrier set up by a rapidly rotating magnetosphere (see Section 2.3.2).

2.3.2 Accretion onto a highly magnetized neutron star

The high magnetic fields of X-ray pulsars further complicate the physics regarding the process of accretion. In the case of the presence of an accretion disk, once the accreting matter gets close enough to the neutron star, the high magnetic field strength will begin to dominate the flow of matter, effectively disrupting the accretion disk. At a critical point, known as the magnetospheric radius, the accretion disk becomes truncated and the accreting matter is driven along the magnetic field lines towards the magnetic poles of the neutron star. The actual dynamics of the flow depends on a variety of factors, but the interaction of matter accreting onto a magnetized neutron star is usually described using an ideal MHD approximation [22]. According to this approximation, the accreting flow of matter is significantly disrupted by the magnetic field of the neutron star at the radius determined by equating the ram pressure of the accreting matter and the magnetic pressure of the dipole field. This radius is known as the Alfvén radius, r_A. For a spherically symmetric mass accretion flow characterized by a mass accretion rate $\dot{M}$ onto a neutron star of mass M_* and magnetic dipole moment μ, r_A is given by:

$$r_A = \left(\frac{\mu^4}{2GM_*\dot{M}^2} \right)^{1/7}, \tag{12}$$

where $\mu = BR_*^3/2$ is the magnetic dipole moment [24][44], and R_* and B is the radius and magnetic field strength of the neutron star, respectively [22]. For example, r_A should be greater than the neutron star's radius in order to show pulsed X-ray emission, which generally requires $B > 10^8$ G. Equation 12 is a useful reference

formula to which the actual value of the boundary of the magnetosphere, the **magnetospheric radius** $r_m = \xi r_A$, can be normalized. The coefficient ξ depends on the configuration of the mass accretion flow: $\xi \sim 1$ for quasi-spherical accretion from a stellar wind [45], while $\xi \sim 0.5$ in the case of disk accretion [46]. The coefficient ξ is generally a function of $\dot{M}$, μ and other parameters [47]. The equation $r_m = \xi r_A$ can be rewritten in the following form:

$$r_m \simeq 2.5 \times 10^8 \xi M_{1.4}^{1/7} R_6^{10/7} B_{12}^{4/7} L_{37}^{-2/7} \ \ [\mathrm{cm}], \tag{13}$$

where R_6 is the radius in units of 10^6 cm, B_{12} is the magnetic field strength in units of 10^{12} G, and L_{37} is the observed luminosity in units of 10^{37} erg/s.

Interactions between the accreting material and the magnetic field lines may lead to torques being exerted on the neutron star. According to the model by Ghosh and Lamb [46], the matter in the accretion disk is threaded by the magnetic field lines, which become twisted by the inflowing plasma as a result of the differential rotation between the neutron star and the accretion disk (see Figure 5). This causes a torque that can either spin-up or spin-down the neutron star. To a first approximation, the torque that is delivered to the neutron star depends on the magnetospheric radius, r_m, as well as the **corotation radius**, r_{co}:

$$r_{co} = \left(\frac{G M_* P^2}{4\pi^2} \right)^{1/3} \simeq 1.68 \times 10^8 M_{1.4}^{1/3} P^{2/3} \ \ [\mathrm{cm}], \tag{14}$$

at which orbiting material in the disk corotates with the neutron star (here P is the spin period of the neutron star in seconds). Material in Keplerian orbits outside of r_{co}, that interacts with the neutron star via the magnetic field, exerts a braking torque on the star, while material in Keplerian orbits inside r_{co} interacting with the neutron star speeds it up.

Because of the fact that r_m increases with decreasing mass accretion rates, it is possible for the magnetospheric radius to reach the corotation radius at some stage. As the mass accretion rate decreases, the ram pressure exerted by accreting matter

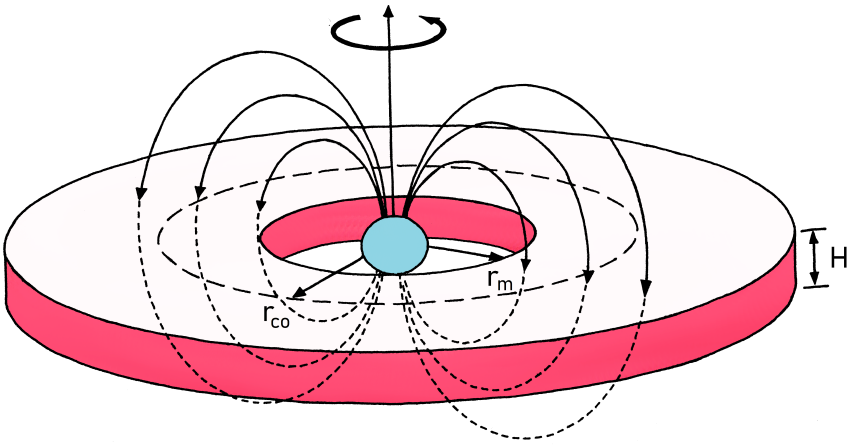

Figure 5. Simplified view of an accretion disk threaded by the magnetic field lines of the neutron star. The schematic shows the truncation of the accretion disk at the magnetospheric radius r_m, and the corotational radius r_{co} where the material in the disk rotates at the same rate as the neutron star. The figure is recreated from Khajenabi et al. 2008 [48].

decreases as well, allowing the magnetosphere to expand. As the magnetosphere expands due to exceedingly low mass accretion rates, it may reach a critical point at which accretion is suddenly stopped by the centrifugal barrier created by the neutron star's fast-rotating magnetosphere. This fascinating phenomenon is known as the **"propeller effect"** (or propeller regime), since the accreting matter is ejected due to the presence of a rapidly rotating magnetosphere [49]. If the magnetospheric radius expands too much, the matter will be flung out by the centrifugal barrier created by the magnetosphere. This happens when the magnetospheric radius overtakes the corotation radius, setting up the following conditions:

$$\begin{cases} \text{if } r_m < r_{co} \Rightarrow \text{accretion is possible.} \\ \text{if } r_m > r_{co} \Rightarrow \text{accretion is prohibited due to the centrifugal barrier.} \end{cases}$$

The limiting luminosity for the onset of the propeller regime can be estimated by equating the corotation radius, r_{co} (Equation 14), with the magnetospheric radius, r_m (Equation 13)[50]:

$$L_{prop} \simeq 4 \times 10^{37} \xi^{7/2} B_{12}^2 P^{-7/3} M_{1.4}^{-2/3} R_6^5 \ \text{[erg/s]}. \tag{15}$$

When r_m starts to exceed r_{co}, an abrupt drop in the luminosity of the source is expected (or a transition into unsteady accretion with large swings in luminosities [32]). Observations of such drops in the luminosity (which have been attributed to the propeller effect) have been reported for several accreting neutron stars, with magnetic fields $B \sim 10^{8-14}$ G [32][50][51].

It is generally believed that all X-ray pulsars transition into the propeller regime if their luminosity drops to L_{prop}. However, recent studies have shown that if the X-ray pulsar exhibits a longer spin period than some critical value for a given magnetic field strength, it will be able to avoid entering the propeller regime, and instead begin to accrete from a cold recombined accretion disk (see section 2.3.1) [42].

2.3.3 X-ray spectrum

The formation of the spectra of accreting X-ray pulsars originate from a hot plasma ($T \sim 10^8$ K) over the magnetic poles of the neutron star. As the inflow of accreted matter is funneled along the magnetic field lines, ultimately falling onto the surface of the neutron star, it forms two roughly column-shaped structures referred to as "accretion columns" [52]. The bulk of the energy of accreted matter that falls onto the small regions around the magnetic poles should be released primarily as X-ray radiation of the accretion columns. However, the observed spectra of accreting X-ray pulsars are notably different from what is expected of blackbody radiation. Instead, the X-ray spectra are typically characterized by a power law ($dN/dE \propto E^{-\Gamma}$) with a photon index, $\Gamma \sim 1$, up to a high-energy cutoff at $10 - 30$ keV, above which the spectrum decays exponentially [32]. This spectral shape is indicative of

Comptonization processes (bulk and thermal) acting on bremsstrahlung, blackbody, and cyclotron seed photons [53].

The high-energy X-ray spectra of several accreting X-ray pulsars show absorption-like features at energies from ~ 10 keV to ~ 100 keV [54]. These features are due to cyclotron resonant scattering of the outgoing radiation by electrons in strong magnetic fields and are referred to as cyclotron resonant scattering features (CRSFs), or **cyclotron lines** [32]. Cyclotron lines are formed close to the magnetic poles of accreting neutron stars with strong magnetic fields ($B \sim 10^{12-13}$ G). The kinetic energies of electrons in such strong magnetic fields are quantized into discrete Landau levels with respect to their motion perpendicular to the magnetic field [52][55], where the energy difference between adjacent Landau levels is given by:

$$E_{Landau} = \hbar\omega_c = \hbar\frac{eB}{m_e c}, \tag{16}$$

where ω_c is the cyclotron frequency, e is the electron charge, B is the magnetic field in the scattering region, m_e is the mass of the electron, and c is the speed of light.

The cyclotron line energies are determined by the separation of the quantized Landau energy levels of electrons, which, in a magnetic field of strength B, are given by [32]:

$$E_{cyc} = E_{Landau}\frac{n}{1+z} \approx \frac{n}{1+z} 11.6 \times B_{12}\ [\text{keV}], \tag{17}$$

where z is the gravitational redshift due to the strong gravitational field around the neutron star, and n is the number of Landau levels involved; $n = 1$ is the case of scattering from the ground level to the first excited Landau level [54]. The resulting cyclotron line is called the fundamental line, and for $n = 2, 3, ...$ the resulting lines are called the first harmonic, second harmonic, and so on. The measurement of cyclotron lines in the X-ray spectra of highly magnetized accreting neutron stars is a powerful tool, as it is the only direct way to measure the magnetic field strength close to the surface of the neutron star [22].

Cyclotron lines were first discovered in the X-ray spectrum of Her X-1 in 1976 [56], providing the first direct measurement of the magnetic field strength of a neutron star. Since the initial discovery, cyclotron lines have been observed in several sources, with a few exhibiting a fundamental line plus harmonics in their X-ray spectra. Many sources also show cyclotron line energy variations as a function of the pulse phase, time and flux [32]. For a recent review on cyclotron lines in neutron stars with high magnetic field strengths, see [54].

In addition to cyclotron lines, several X-ray pulsars also exhibit the Fe K_α fluorescence emission line at ~ 6.4 keV, presumably produced when the X-ray emission from the central pulsar irradiates the surrounding material, which can be either the stellar wind or the accretion disk [57].

3 Methods

3.1 Overview of the Swift Observatory

The Neil Gehrels Swift Observatory (*Swift*) [58] is a multi-wavelength observatory dedicated to studying the science of gamma-ray bursts (GRBs). Although this was the main focus of *Swift*, it now serves as a general purpose multi-wavelength observatory and is used to study other sources of X-rays and gamma-rays, e.g., X-ray binaries. Observations of X-ray binaries can be triggered by some unusual event, such as an outburst. *Swift* is part of NASA's medium explorer (MIDEX) program and was launched into a low-Earth orbit (LEO) on a Delta 7320 rocket on November 20, 2004. The instruments were developed by an international team from the US, the UK, and Italy, with additional scientific involvement in France, Japan, Germany, Denmark, Spain, and South Africa. The *Swift* telescope payload is comprised of three instruments utilized together to observe transient astrophysical phenomena in the gamma-ray, X-ray, and optical wavebands. These instruments work in tandem to provide fast characterization and multi-wavelength follow-up of all kinds of astrophysical transients, in addition to GRBs and their afterglows.

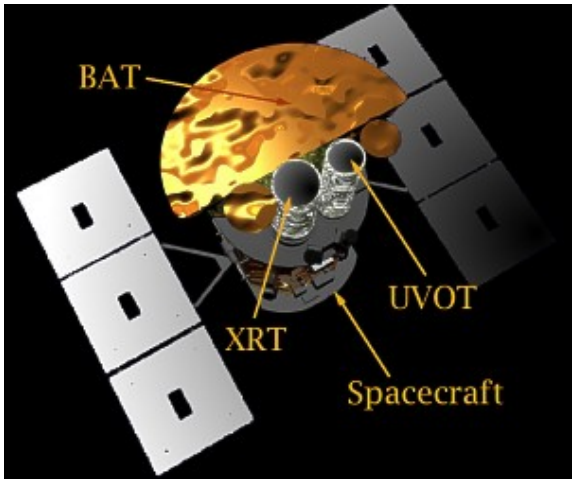

Figure 6. *Swift* Observatory. BAT - Burst Alert Telescope; XRT - X-ray Telescope; UVOT - UV/Optical Telescope. Image credit: https://www.swift.psu.edu/

The **Burst Alert Telescope** (BAT) has a large field-of-view (FOV) and high sensitivity, covering a large fraction of the sky. It is able to detect and compute the positions of transient events on-board the satellite with arc-minute positional accuracy. The **X-ray Telescope** (XRT) takes images and is able to obtain spectra of sources during pointed follow-up observations. The images are used for higher accuracy position localizations. The XRT is also used for long-term monitoring of the light curves of sources for days to weeks after a transient event, depending on the brightness of the afterglow. The **UV/Optical Telescope** (UVOT), operating in the optical band (170-600 nm), takes images and can obtain spectra of sources during pointed follow-up observations. The images are used for 0.5 arcsec position localizations and for following the temporal evolution of the UV/optical afterglow.

3.1.1 Swift/BAT

The *Swift*/BAT is a highly sensitive and large FOV instrument, designed to provide critical triggers for transient events and 4 arcmin positions. It is a coded aperture imaging instrument with a 1.4 steradian FOV (half coded). The energy range is 15-150 keV for imaging with a non-coded response up to 500 keV [59][60]. *Swift* utilizes momentum wheels to autonomously slew into the direction of transient events. Within several seconds of detecting an event, the BAT calculates an initial position, decides whether the burst merits a spacecraft slew and, if so, sends the position to the spacecraft. In order to study events with a variety of intensities, durations, and temporal structures, the BAT must have a large dynamic range and trigger capabilities. The BAT uses a 2D coded aperture mask and a large solid state detector (SSD) array to detect weak outbursts, and has a large FOV to detect a good fraction of bright bursts. Since the BAT coded aperture FOV always includes the XRT and UVOT FOVs, long duration gamma-ray emission from bursts can be studied simultaneously with X-ray and UV/optical emission. The data from the BAT is

also able to produce a sensitive hard X-ray all-sky survey over the course of *Swift*'s mission, as well as work as a monitor for X-ray transients[7]. Table I lists the most important parameters of the BAT. The BAT runs in two modes: burst mode, which produces burst positions, and survey mode, which produces hard X-ray survey data. In survey mode, the instrument collects count-rate data in five-minute time bins for 80 energy intervals. When a burst occurs it switches into a photon-by-photon mode with a ring-buffer to save pre-burst information.

Table I. *BAT* instrument parameters.

Property	**Description**
Aperture	Coded mask
Detecting Area	5200 cm^2
Detector	Cadmium Zinc Telluride (CdZnTe)
Detector Operation	Photon Counting
Field-of-View	1.4 sr (partially-coded)
Detection Elements	256 modules of 128 elements
Detector Size	4 mm × 4 mm × 2 mmm
Telescope PSF	17 arcmin
Energy Range	15-150 keV

3.1.2 Swift/XRT

The *Swift*/XRT is a sensitive, flexible, autonomous X-ray CCD (Charged Coupled Device) imaging spectrometer designed to measure the position, spectrum, and brightness of outbursts over a wide dynamic range covering more than 7 orders of magnitude in flux. Table II summarizes the parameters of the instrument. Further information on the XRT is given by [61]. The XRT is a focusing X-ray telescope with

[7]See `https://swift.gsfc.nasa.gov/results/transients/` for the Swift/BAT Hard X-ray Transient Monitor data.

a 110 cm^2 effective area, 23.6 × 23.6 arcmin FOV, 18 arcsec resolution (half-power diameter), and 0.2-10 keV energy range. The XRT uses a grazing incidence Wolter Type I telescope (with 12 nested mirrors) to focus X-rays onto a state-of-the-art CCD. The CCD consists of an image area with 600 × 602 pixels (40 × 40 microns) and a storage region of 600 × 602 pixels (39 × 12 microns).

Table II. *XRT* instrument parameters.

Property	**Description**
Telescope	JET-X Wolter I
Focal Length	3.5 m
Effective Area	100 cm^2 at 1.5 keV
Telescope PSF	18 arcsec HPD at 1.5 keV
Detector	EEV CCD-22, 600 × 600 pixels
Detector Operation	Imaging, Timing and Photon-counting
Detection Element	40 × 40 micron pixels
Pixel Scale	2.36 arcsec/pixel
Energy Range	0.2-10 keV
Sensitivity	8×10^{-14} erg cm^{-2} s^{-1} in 10^4 seconds

The XRT supports three readout modes to enable it to cover the dynamic range and rapid variability of X-ray sources. On-board software autonomously determines which readout mode to use for each source, based on the measured count rate. The **Imaging Mode** produces an integrated image measuring the total energy deposited per pixel and does not permit spectroscopy, so it will only be used to position bright sources. The **Timing Mode** sacrifices position information to achieve high time resolution and bright source spectroscopy through rapid CCD readouts. The **Photon-counting Mode** uses sub-array windows to permit full spectral and spatial information to be obtained for source fluxes ranging from the XRT sensitivity limit of 2×10^{-14} to 9×10^{-10} erg cm^{-2} s^{-1}.

3.2 Data reduction and analysis

For the analysis, data obtained from observations with both the BAT and XRT instruments on-board the *Swift* observatory were used. For all of the sources in this work (SMC X-2, V 0332+53, 4U 0115+63, GRO J1008–57), *Swift*/XRT observations corresponding to known outbursts were chosen to study the luminosity decay into quiescence. Each observation's spectrum was then created using the online tools provided by the UK Swift Science Data Centre [62][8].

It is general practice to use the method of forward-fitting for spectral analysis in X-ray astronomy. This is comprised of defining and calculating a spectral model, which is convolved with the response of the detector and thereafter compared to the actual observed data. The parameters of the spectral model are modified until the best fit is achieved; this is evaluated by the use of some form of statistic. The spectral model chosen should always be physically motivated based on knowledge of the source under consideration. For the analysis in this work, spectra were grouped to have at least one count per energy bin and were fitted with the XSPEC package (which is the standard package for X-ray spectral analysis included in NASA's HEASOFT software suite) using the C-statistic [63]. To avoid any problems caused by calibration uncertainties at low energies,[9] the spectral analysis was kept within the 0.7-10 keV band. In order to account for the effect of absorption in the interstellar medium and calculate the unabsorbed flux of the sources, the CFLUX routine from the XSPEC package was used. More details of the data analysis for each individual source are described in Section 3.3, specifically information about which spectral model and bolometric correction factor was used.

Swift/BAT Hard X-ray Transient Monitor data is available online (`https://swift.gsfc.nasa.gov/results/transients/`) and was downloaded for SMC X-2, V 0332+53, and 4U 0115+63 in order to create the long-term light curves in

[8] `http://www.swift.ac.uk/user_objects/`

[9] `http://www.swift.ac.uk/analysis/xrt/digest_cal.php`

the bright state (see Figures 8-11). In order to convert the count rate from the *Swift*/BAT data to the source flux, it is useful to utilize the average Crab rate in the BAT 15-50 keV band as a yardstick [64]. For the BAT 15–50 keV band, 1 mCrab is equal to about 0.00022 counts/cm^2/s, which (using a power law with a photon index of $\Gamma = 2.15$ [65]) corresponds to 1.26×10^{-11} erg/cm^2/s. The comparison of the source flux to Crab flux is true only for sources with the same photon index, however, the systematic error for sources with different indices is small [64].

In order to produce the light curves of the sources, the flux of each observation was converted to the luminosity. The luminosity L_X was calculated from the unabsorbed flux derived from the *Swift*/XRT data and the flux derived from the count rate of the *Swift*/BAT data, assuming:

$$L_X = F \times 4\pi d^2, \tag{18}$$

where F is the flux and d is the distance to the source. In order to discuss the properties of the outbursts of the selected sources, a bolometric correction was applied to the determined luminosities for all *Swift*/XRT data. For a bolometric correction factor K_{bol}, the bolometric luminosity is simply given by:

$$L_{bol} = K_{bol} \times L_X. \tag{19}$$

The next step of the analysis involved fitting the *Swift*/XRT light curves. The light curves of the sources were smoothed using LOWESS (Locally Weighted Scatterplot Smoothing) [66], by using the implementation provided by the Python library statsmodels. The resulting data points from the smoothing procedure were then fitted with a 1-D smoothing spline using Scipy, a Python library used for scientific and technical computing. By using a smoothing filter such as LOWESS, the overall long-term behavior of the light curves of the individual sources can be described, without catching as much of the small-term variations which are not of interest for this particular analysis (see Figure 7 for an example of the use of LOWESS).

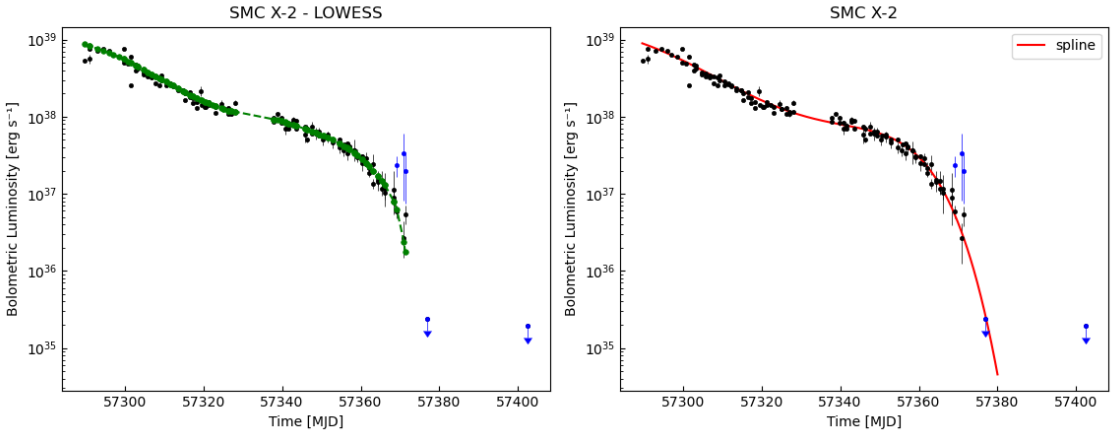

Figure 7. *Left:* The process of applying LOWESS to the light curve of SMC X-2 is illustrated, where the green dots are the smoothed data points, black dots are the original data points, and blue dots are the data points excluded from the smoothing procedure. *Right:* The fitting procedure of SMC X-2 is shown, where the red line is the fitted curve produced by using a spline of degree k=5.

3.3 Sample of individual sources

In this section the main observational characteristics of each individual source are mentioned, including spin and orbital period, distance, and magnetic field strength, as well as detected cyclotron lines. The most important properties are summarized in table III. In addition to this, specific details about the analysis of each individual source are described. Figures 8-11 show the *Swift*/BAT light-curves of the sample of sources in the 15-50 keV energy range, displaying their characteristic transient behavior.

SMC X-2

SMC X-2 is one of the brightest X-ray pulsars in the Small Magellanic Cloud[10], with a maximum detected luminosity of $L_X = 4 \times 10^{38}$ erg/s. SMC X-2, which is categorized as a transient BeXB, was discovered during a Type II outburst by *SAS-3* in 1977 [68] and exhibits a spin period of $P_{spin} \approx 2.37$ s [69][70]. Observations by

[10]The Small Magellanic Cloud (SMC) is a satellite galaxy of the Milky Way, located at a distance of $d \approx 62$ kpc [67], that is extremely rich in BeXBs.

the OGLE experiment revealed the variability of an early spectral type star close to the X-ray position of SMC X-2, with a period of $P_{orb} = 18.62 \pm 0.02$ days [71] in line with periodic variations detected by the *RXTE* and *Swift* observatories at $P_{orb} \approx 18.4$ days [72][73]. This periodicity has been interpreted as the orbital period of the binary system, which combined with the spin period classifies SMC X-2 as a BeXB. *NuSTAR* data from the outburst in 2015 suggests the existence of a cyclotron line in its spectrum at ~ 27 keV [74].

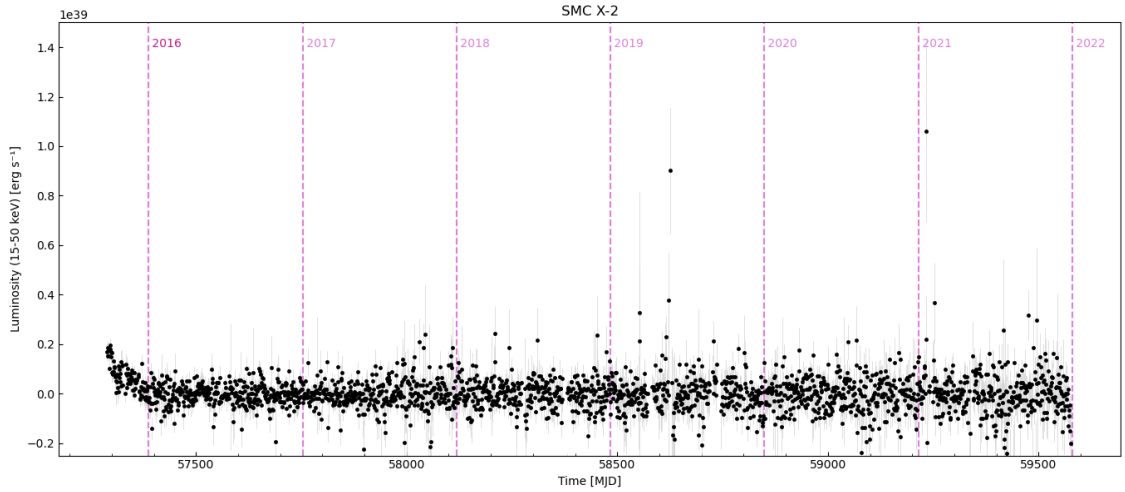

Figure 8. The evolution of the luminosity of SMC X-2 based on observations made by the *Swift*/BAT telescope.

The observations used for the analysis of SMC X-2 in this thesis were performed by the *Swift*/XRT telescope after the X-ray pulsar entered an outburst in September 2015, more specifically between MJD 57289 and MJD 57412. The observations made by the *Swift*/XRT telescope were performed in both the WT (Windowed Timing) and PC (Photon Counting) modes, depending on the brightness of the source. The spectral fitting procedure follows the model of Lutovinov et al. [51]. The spectra in the high state (i.e., at high luminosities) of the source can be well fitted with a power-law model modified by interstellar absorption (PHABS-component) at low energies (PHABS*POWERLAW in the XSPEC package). The hydrogen column density was fixed at $N_H = 3.4 \times 10^{21}$ cm^{-2} for the fitting procedure. The bolometric luminosity

was calculated from the unabsorbed flux assuming a distance of $d = 62$ kpc and a bolometric correction factor of $K_{bol} = 2.5$.

In the low state (i.e., at low luminosities), the source was not detected in any single observation, and therefore multiple observations were averaged into two groups according to the dates of the observations [51]. Analysis of the image of each respective group was done using an aperture of 18" radius centered at the source position in order to get the source counts. A much larger area was subsequently used to estimate the background count rate, defined by an annulus centered at the source position with inner and outer radii of 70" and 250", respectively. The background count rate was then re-scaled according to the number of counts expected within the aperture of the source. In order to convert the count rate into flux, the same procedure was repeated for an observation in the high-state, giving the net count rate. By assuming the same spectral shape in both the high and low state, the flux level in the low state was determined from re-scaling of the corresponding count rates, resulting in the upper limits for the two averaged groups.

4U 0115+63

4U 0115+63 was discovered as an X-ray source by the *UHURU* observatory in the early 1970s [75][76]. X-ray pulsations at a period of $P_{spin} = 3.61$ s were found during *SAS-3* observations in 1978 [77] and the orbital period $P_{orb} = 24.3$ d was estimated by Rappaport et al. [78] in 1978 using the *SAS-3* data. Optical observations allowed for the star V635 Cas to be identified as the stellar companion of 4U 0115+63 [79], and in-depth studies found the distance to the binary system to be ~ 7 kpc, and allowed for the improvement of the spectral type of the star, B0.2Ve [80]. 4U 0115+63 shows transient behavior, including giant Type II outbursts occurring regularly every three years or so [81]. In 1980, a cyclotron line at ~ 20 keV was discovered in its spectrum using data obtained by *HEAO-1*/A4 [82]. However, a closer look at the

data revealed the existence of a pair of line features at 11.5 keV and 23 keV, which were interpreted as the fundamental line plus the first harmonic [83]. This X-ray pulsar holds the record for number of harmonics, being the only object where cyclotron lines have been detected in its spectrum up to the fifth harmonic [84][85][86].

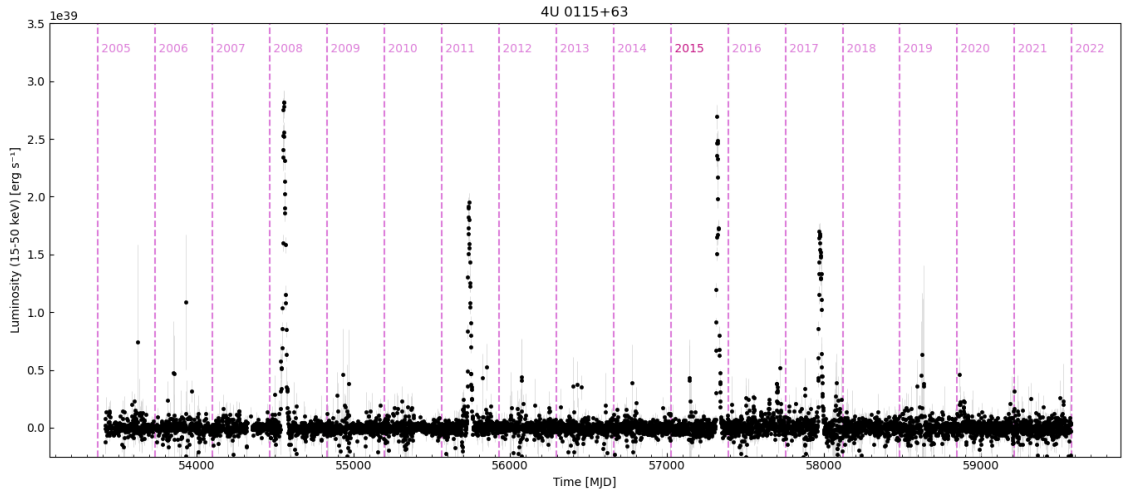

Figure 9. The evolution of the luminosity of 4U 0115+63 based on observations made by the *Swift*/BAT telescope.

The observations used for the analysis of 4U 0115+63 were performed covering the declining phases of the giant Type II outburst in 2015 between MJD 57329 and MJD 57388. The *Swift*/XRT observations were made in both PC and WT mode depending on the brightness of the source. The spectral fitting procedure follows the model of Tsygankov et al. [50]. The spectra in the 0.5-10 keV range of 4U 0115+63 in the high state can be described by an absorbed power-law model (PHABS*POWERLAW in the XSPEC package). To fit the spectra in the low state, an absorbed black-body model (PHABS*BBODYRAD in the XSPEC package) with a free black-body temperature and a fixed hydrogen column density of $N_H = 1.1 \times 10^{22}$ cm^{-2} (the average value in the high state) was used. The bolometric luminosity in the high state was calculated from the unabsorbed flux assuming a distance of $d = 7$ kpc and a bolometric correction factor of $K_{bol} = 2$.

V 0332+53

V 0332+53 was discovered as a transient X-ray source during an outburst in 1973 by the Vela 5B satellite [87]. Subsequent outbursts in 1983-1984 and 1989 observed with the *EXOSAT* and *Ginga* observatories led to the determination of the spin period $P_{spin} \sim 4.4$ s, and orbital period $P_{orb} \sim 34.25$ d of this bright X-ray pulsar [88]. The stellar companion of V 0332+53, BQ Cam, is a Be star of spectral class O8-9Ve located at an estimated distance of ~ 7 kpc [89]. A cyclotron line has been identified in the source's spectrum with a line energy of $E_{cyc} = 28.5 \pm 0.5$ keV [90]. V 0332+53 exhibits both Type I and giant Type II outbursts, which is typical for Be systems, with luminosities peaking at around $\sim 10^{37-38}$ erg/s, making it one of the brightest X-ray sources in our Galaxy.

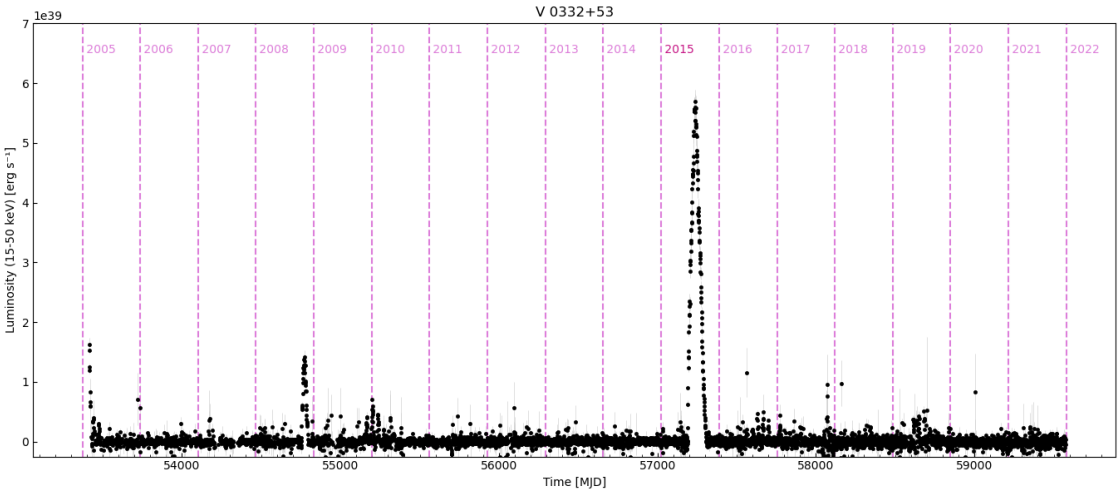

Figure 10. The evolution of the luminosity of V 0332+53 based on observations made by the *Swift*/BAT telescope.

The observations used for the analysis of V 0332+53 were performed covering the declining phase of the giant Type II outburst in 2015, specifically between MJD 57293 and MJD 57393. The *Swift*/XRT observations were made in both PC and WT mode depending on the brightness. The spectral fitting procedure follows the model of Tsygankov et al. [50]. In the high state, the spectra of V 0332+53 can be well described by an absorbed power-law model (PHABS*POWERLAW in the

XSPEC package). To fit the spectra in the low state, an absorbed black-body model (PHABS*BBODYRAD in the XSPEC package) with a free black-body temperature and a fixed hydrogen column density of $N_H = 1.2 \times 10^{22}$ cm^{-2} (the average value in the high state) was used. The bolometric luminosity in the high state was calculated from the unabsorbed flux assuming a distance of $d = 7$ kpc and a bolometric correction factor of $K_{bol} = 2$.

GRO J1008–57

GRO J1008–57 was discovered as an X-ray pulsar by the Compton Gamma-Ray Observatory's (*CGRO*) BATSE instrument during an outburst in 1993, which found the neutron star rotating with period of $P_{spin} = 93.587 \pm 0.005$ s [91]. GRO J1008–57 is a transient BeXB with a stellar companion of type B1-B2 Ve [92], located at a distance of ~ 5 kpc [93], showing regular Type I and giant Type II outbursts. Based on *RXTE*-ASM data, an orbital period of $P_{orb} = 249.46 \pm 0.10$ d was determined by Levine and Corbet in 2006 [94]. A cyclotron line at $E_{cyc} = 75.5$ keV was discovered in the spectrum of the source with *Suzaku* [95], confirming the earlier suggestion of the spectral feature at ~ 88 keV based on *CGRO*/OSSO data [96].

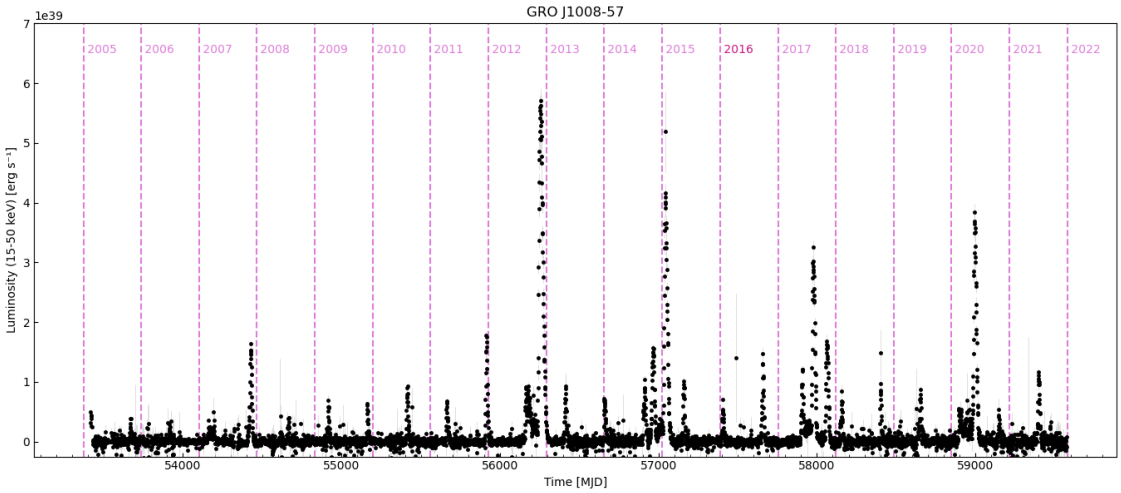

Figure 11. The evolution of the luminosity of GRO J1008–57 based on observations made by the *Swift*/BAT telescope.

The observations used for the analysis of GRO J1008–57 were made by the *Swift*/XRT telescope during two consecutive Type I outbursts in January and September 2016, between MJD 57402 and MJD 57648. The observations were performed every 3-4 days in PC mode. The spectral fitting procedure follows Tsygankov et al. [42]. The spectra from all individual observations were fitted with a simple power-law model modified by interstellar absorption at low energies (PHABS*POWERLAW in the XSPEC package). The hydrogen column density was fixed at $N_H = 2.0 \times 10^{22}$ cm^{-2}. The bolometric luminosity was calculated from the unabsorbed flux assuming a distance of $d = 5.8$ kpc and a bolometric correction factor of $K_{bol} = 1.6$. The behavior of the light-curve of GR0 J1008–57 (see Figure 16 has been proposed to be the result of the system transitioning into the stable regime of accretion from a cold recombined disk (see [42]).

Table III: Sample of individual sources.

Source name	RA (J2000)	DEC (J2000)	Optical Comp.	Spec.type	P_{spin} (s)	P_{orb} (d)	d (kpc)	E_{cyc} (keV)	B_{12} from E_{cyc} (10^{12} G)
GRO J1008–57	152.4457	-58.2932	-	B0e	93.59	249.5	5.8	75.5	8.5
V 0332+53	53.7496	53.1731	BQ Cam	O8-9Ve	4.4	34.25	7.0	28	3.1
4U 0115+63	19.6332	63.7425	V635 Cas	B0.2Ve	3.61	24.3	7.0	11.5	1.3
SMC X-2	13.6393	-73.6837	-	-	2.37	18.4	62	27	3.0

4 Results and discussion

The obtained light-curves of the selected sources are found in Figure 13-16. As previously stated (Sections 2.3.1 and 2.3.2), in theory, at the end of an outburst the X-ray pulsar can end up in two different regimes depending on a combination of spin period and magnetic field strength: the stable regime of accretion from a cold, recombined disk, or the propeller regime. In order for the X-ray pulsar to avoid entering the propeller regime and instead transition to the stable cold disk regime, its magnetosphere needs to possess a sufficiently low centrifugal barrier. As can be seen from Equation 15, this will ultimately depend on the strength of the magnetic field B, which affects the extent of the magnetosphere, r_m, and the spin period P, which affects the location of r_{co}. For a given magnetic field strength and spin period, X-ray pulsars can then be divided into two groups: those who display the propeller effect and those who enter the cold disk regime (see Figure 12).

Following the discussion in [42], two conditions need to be met in order for the X-ray pulsar to transition into accreting matter from a cold, recombined disk. Firstly, the mass accretion rate has to be sufficiently high in order to allow matter to penetrate the centrifugal barrier of the magnetosphere, i.e., $r_{co} > r_m$. Secondly, the mass accretion rate also has to be low enough for the temperature of the entire disk to remain at < 6500 K. [42] The second condition requires $\dot{M} < \dot{M}_{cold}$ (see Equation 11). This can simply be expressed in regards to the luminosity corresponding to the transition into the regime of accretion from a cold disk by substituting the magnetospheric radius ($r = r_m$) into Equation 11:

$$L_{cold} = 9 \times 10^{33} k^{1.5} M_{1.4}^{0.28} R_6^{1.57} B_{12}^{0.86} \ \text{[erg/s]}, \tag{20}$$

where for $L < L_{cold}$, the temperature in the accretion disk is lower than 6500 K at $r > r_m$. Therefore, for $L_{prop} < L_{cold}$, the accretion disk will transition into the cold disk accretion regime, which allows for stable mass accretion even at low mass accretion rates.

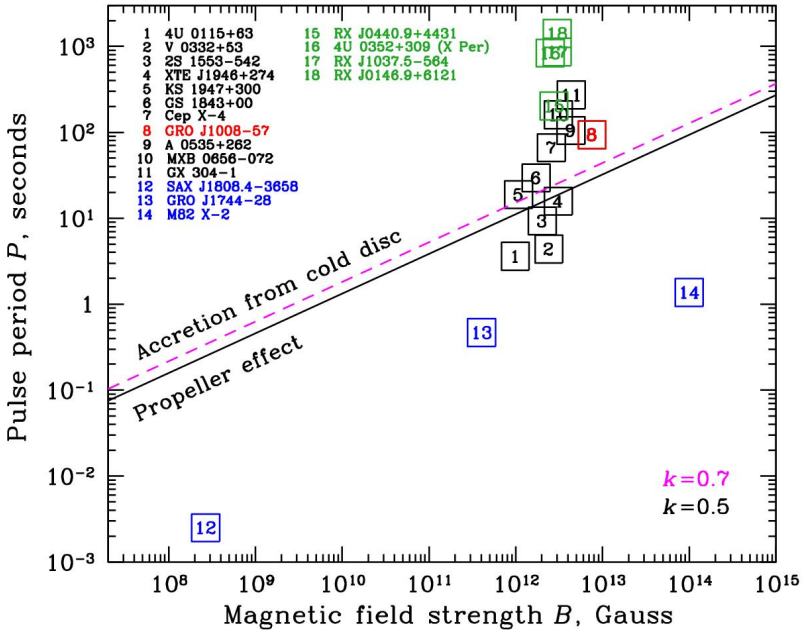

Figure 12. Several known transient BeXBs (in black) and persistent BeXBs (in green) are shown on the $B - P$ plane, and additionally the AMP SAX J1808.4–3658, the bursting pulsar GRO J1744–28, and the ULX M82-2 (in blue). The sources are divided into two areas (propeller regime and cold disk regime) by the line corresponding to $L_{prop} = L_{cold}$ (see Equation (17) [42]). Note that GRO J1008–57 (in red) resides in the region of stable accretion from a cold disk. Figure from Tsygankov et al. [42]

.

In the S-curve, commonly used as an illustration in the DIM, the middle branch represents the unstable region of intermediate mass accretion rates and the transition into this region occurs through a **propagating front**. In the upper left of Figure 4, the decay from outburst is illustrated, which includes the depiction of the propagation of a cooling front, which appears when a temperature of $\sim$ 6500 K is reached at some radius r in the accretion disk. Similarly, a heating front during the rise to the peak of the outburst is depicted in the lower right of Figure 4. The following section (4.1) discusses the properties of propagating fronts in the DIM framework, as well as the application of a cooling front in the context of the transient X-ray pulsars discussed in this work.

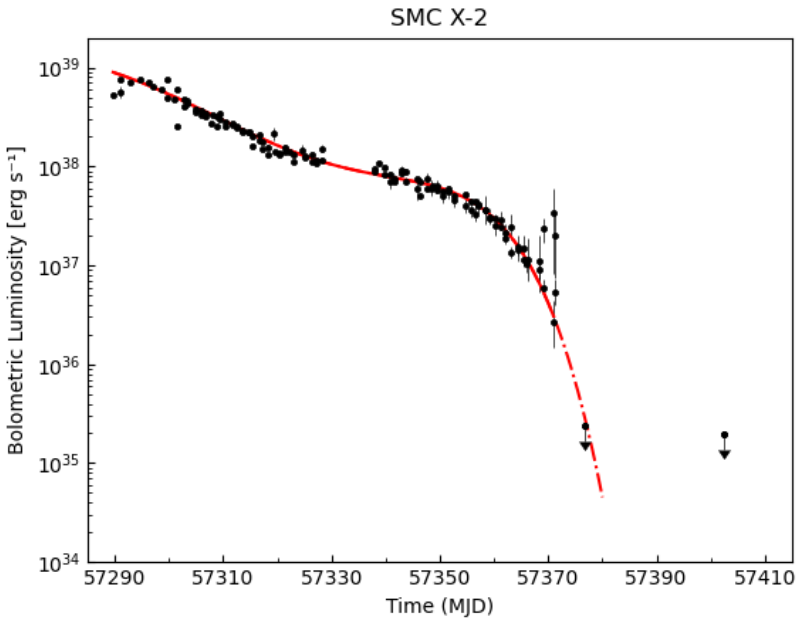

Figure 13. The evolution of the bolometric luminosity of SMC X-2 based on observations made by the *Swift*/XRT telescope. The red line corresponds to the fitted curve produced by using a combination of LOWESS and a spline of degree k=5.

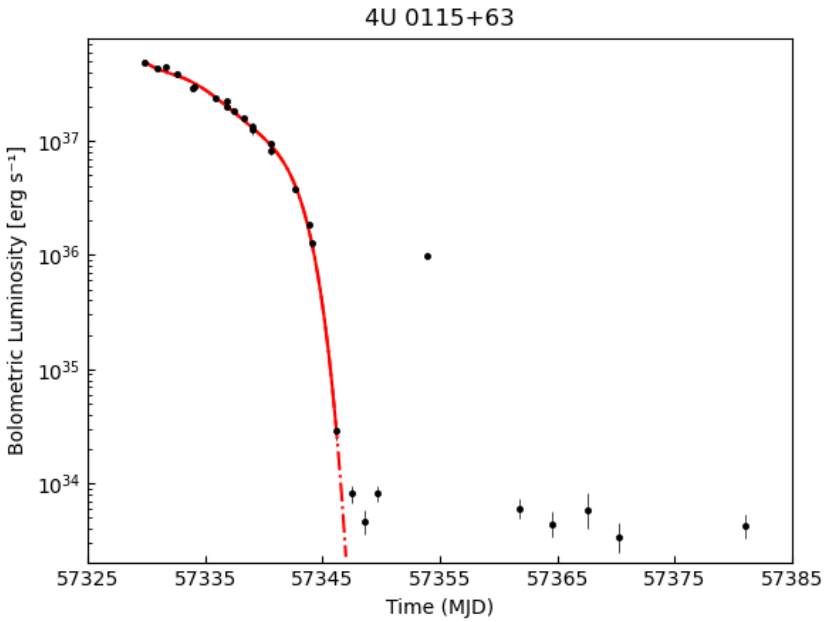

Figure 14. The evolution of the bolometric luminosity of 4U 0115+63 based on observations made by the *Swift*/XRT telescope. The red line corresponds to the fitted curve produced by using a combination of LOWESS and a spline of degree k=5.

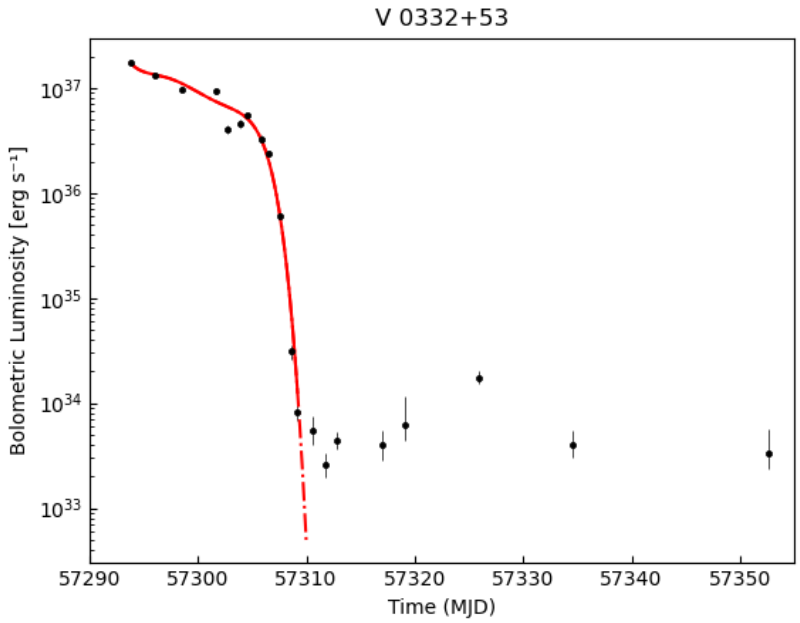

Figure 15. The evolution of the bolometric luminosity of V 0332+53 based on observations made by the *Swift*/XRT telescope. The red line corresponds to the fitted curve produced by using a combination of LOWESS and a spline of degree k=5.

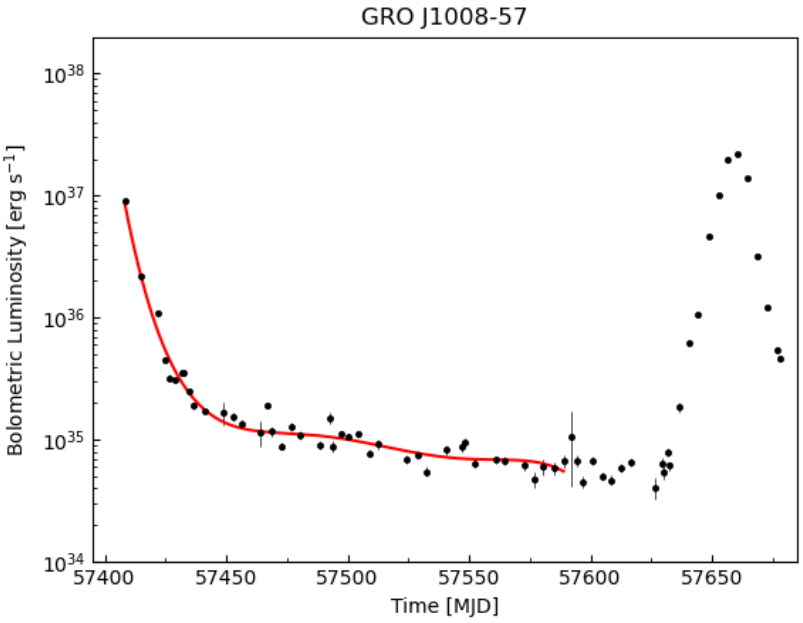

Figure 16. The evolution of the bolometric luminosity of GRO J1008–57 based on observations made by the *Swift*/XRT telescope. The red line corresponds to the fitted curve produced by using a combination of LOWESS and a spline of degree k=5.

4.1 Propagating fronts

As the accretion disk transitions between the hot state and the cold state, which has been triggered at some radial distance r, transition waves or fronts propagate inward or outward, transforming the bi-stable disk region from the hot state to the cold state (or vice versa) [97]. The properties of propagating fronts, or more specifically heating fronts, have been compared to ignition fronts in combustion waves [98], where the ignition front propagates into unburned matter ("cold state") leaving behind burned matter ("hot state"). The combustion wave (the ignited region between the unburned and burned regions) propagates with a certain velocity into the unburned region. Matter inside the propagating front is heated on the burning time scale, subsequently igniting the matter into which it is propagating by heat diffusion. During the burning time τ_b, heat diffuses over a distance $V_{front}\tau_b$ covered by the front during this time, which means that the front speed V_{front} can be written as:

$$V_{front} \approx \frac{\nu_{th}}{\tau_b}, \tag{21}$$

where ν_{th} is the coefficient of thermal diffusion [98]. In accretion disks the thermal diffusivity coefficient (which is the same as the kinematic viscosity coefficient) can be written as:

$$\nu_{th} \approx \frac{H^2}{\tau_{th}}, \tag{22}$$

where $\tau_{th} = (\alpha\Omega_K)^{-1}$, so that the front speed is [41]:

$$V_{front} \approx \alpha c_s. \tag{23}$$

When modeling the outbursts of dwarf novae, two values for α are generally used, as the value is assumed to be different on the hot and cold branches. The ratio $\alpha_{hot}/\alpha_{cold}$ of the hot to cold values is typically of the order of 5–10 and the standard version of the DIM uses $\alpha_{cold} \sim 0.02 - 0.04$ and $\alpha_{hot} \sim 0.1 - 0.2$ [39]. The dependence on α_{cold} is, however, weak and the cooling front velocity is of the order of $\alpha_{hot}c_s$ (slower

by typically a factor of 10 compared to heating fronts)[41].

In order to examine the possibility of the appearance of a cooling front in the X-ray pulsar's accretion disk, the declining phase of the outburst can be approximated by utilizing the decay of the luminosity according to the equation:

$$\sigma T_{eff}^4 = \frac{3}{8\pi}\frac{LR_*}{r^3} \times f, \tag{24}$$

where f is an inner boundary-condition factor (see, e.g., Frank et al. [99]):

$$f = \left[1 - \left(\frac{r_{in}}{r}\right)^{1/2}\right].$$

Equation 24 relates the mass accretion rate $\dot{M}$ (and therefore the luminosity) to the effective temperature T_{eff} in the accretion disk. Equation 24 can be used to give a rough estimate of the radial distance r in the accretion disk where the effective temperature is equal to 6500 K, i.e the radius in the accretion disk at which the cooling front is present. In accordance to the estimates for the velocity of the cooling front, $V_{cold} \approx \alpha_{cold} \times c_s$, the luminosity decrease during the declining phases of the outburst can be then modeled, where α_{cold} is adjusted in order to achieve the closest resemblance to the real observational data. The exact boundary condition is uncertain and for this work either r_{in} is assumed to equal the magnetospheric radius r_m, or $r \ll r_m$. For the latter case, $f = 1$, and the reasonable assumption is made that the true boundary condition lies somewhere in between these two cases.

Figures 17, 18, 19 shows the declining phases of the outbursts of SMC X-2, 4U 0115+63, and V 0332+53, with the fitted spline in red, and the luminosity decay corresponding to the cooling front determined from Equation 24 (blue assuming $f = 1 - \left(\frac{r_{in}}{r}\right)^{1/2}$ and purple assuming $f = 1$). For SMC X-2, 4U 0115+63, and V 0332+53 the approximate values of α_{cold} are: 0.018, 0.040, 0.046, respectively.

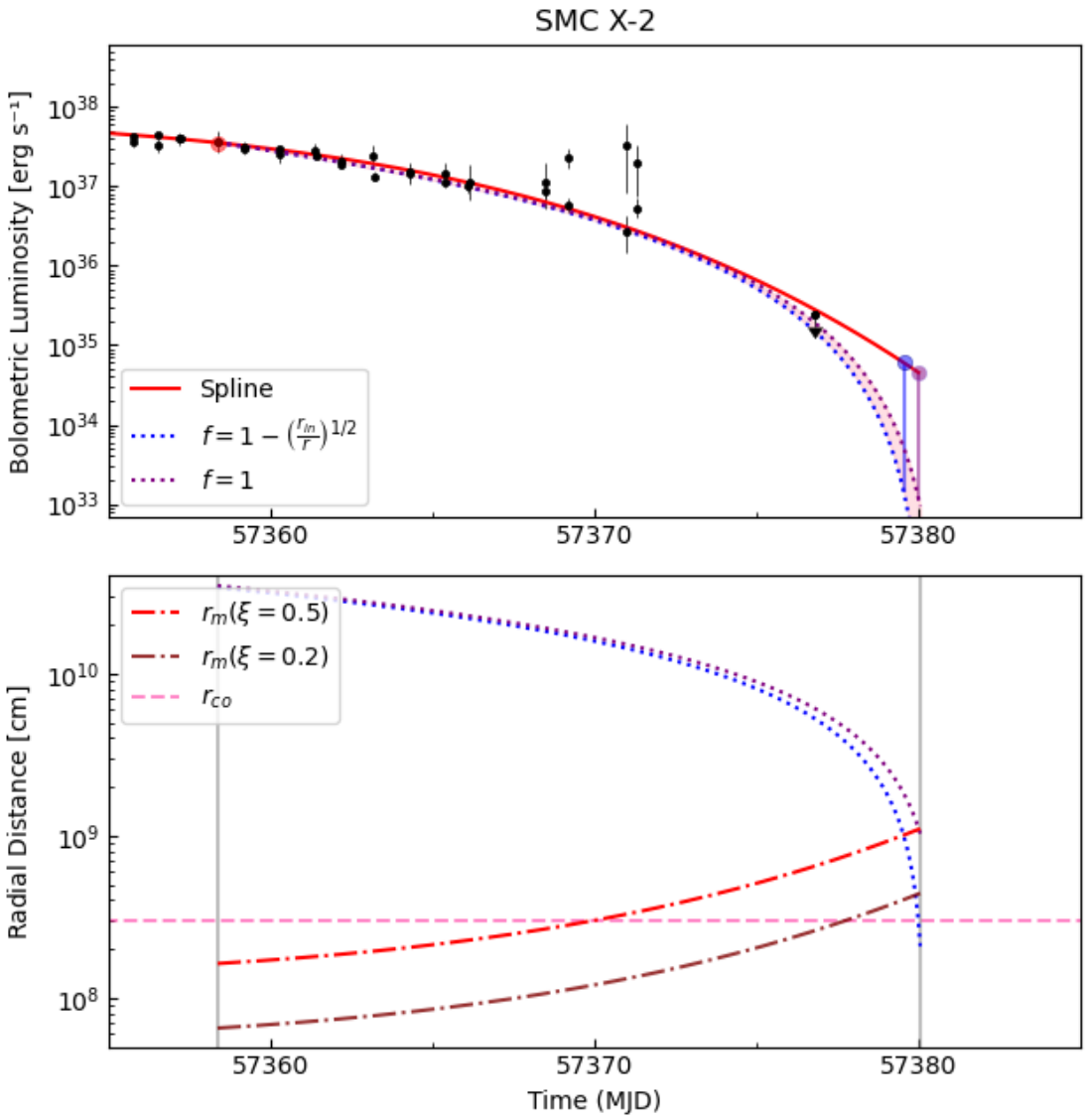

Figure 17. *Top:* The outburst decay of SMC X-2 based on observations made by the *Swift*/XRT telescope. The red line corresponds to the fitted spline, blue and purple corresponds to estimates for the luminosity decay caused by a propagating cooling front. *Bottom:* The evolution of the radial distance of the cooling front compared to the increase in r_m due to decreasing mass accretion rates. The red and brown line corresponds to r_m for $\xi = 0.5$ and $\xi = 0.2$, respectively. The corotation radius r_{co} is shown as a horizontal line (pink).

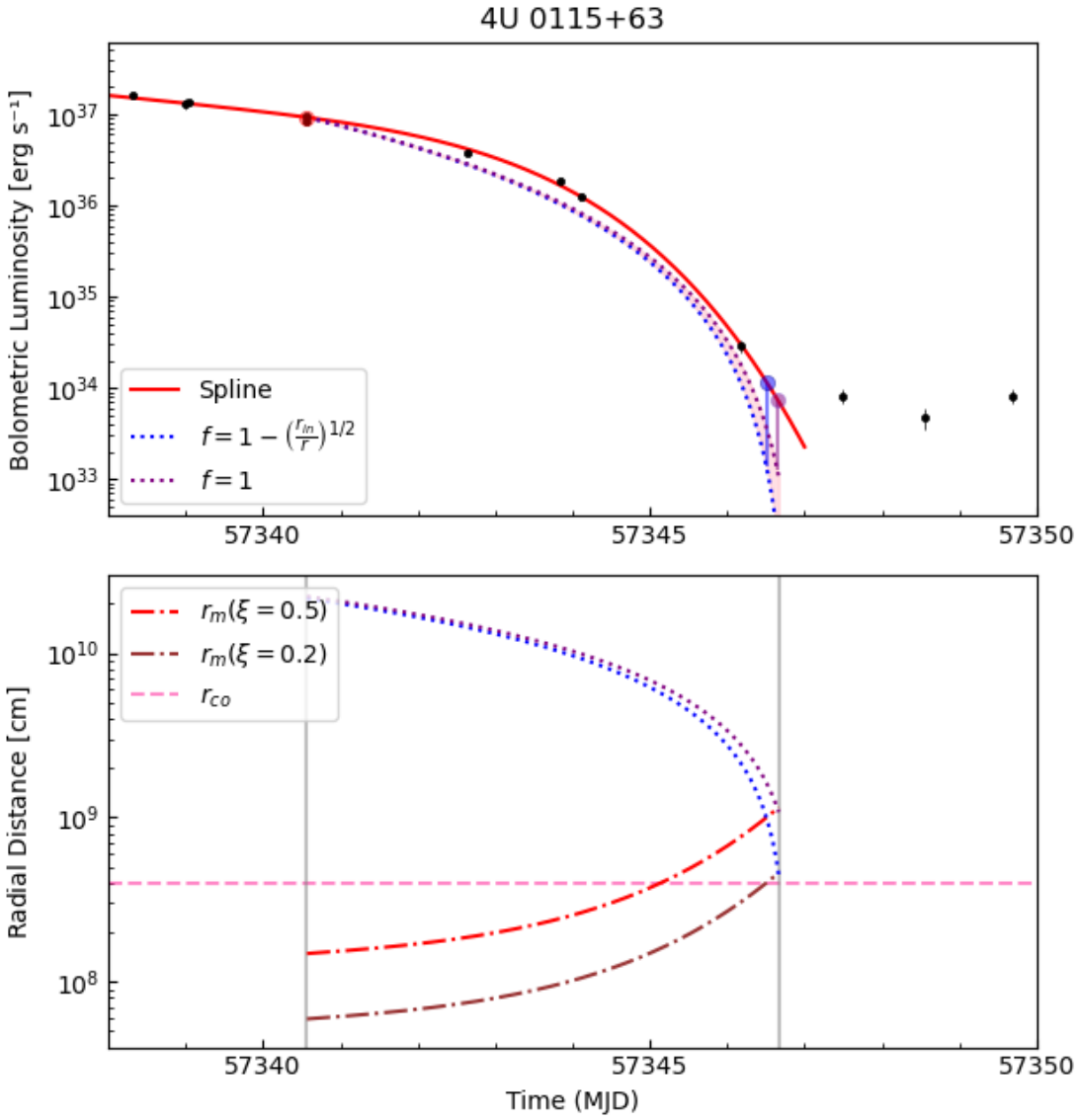

Figure 18. *Top:* The outburst decay of 4U 0115+63 based on observations made by the *Swift*/XRT telescope. The red line corresponds to the fitted spline, blue and purple corresponds to estimates for the luminosity decay caused by a propagating cooling front. *Bottom:* The evolution of the radial distance of the cooling front compared to the increase in r_m due to decreasing mass accretion rates. The red and brown line corresponds to r_m for $\xi = 0.5$ and $\xi = 0.2$, respectively. The corotation radius r_{co} is shown as a horizontal line (pink).

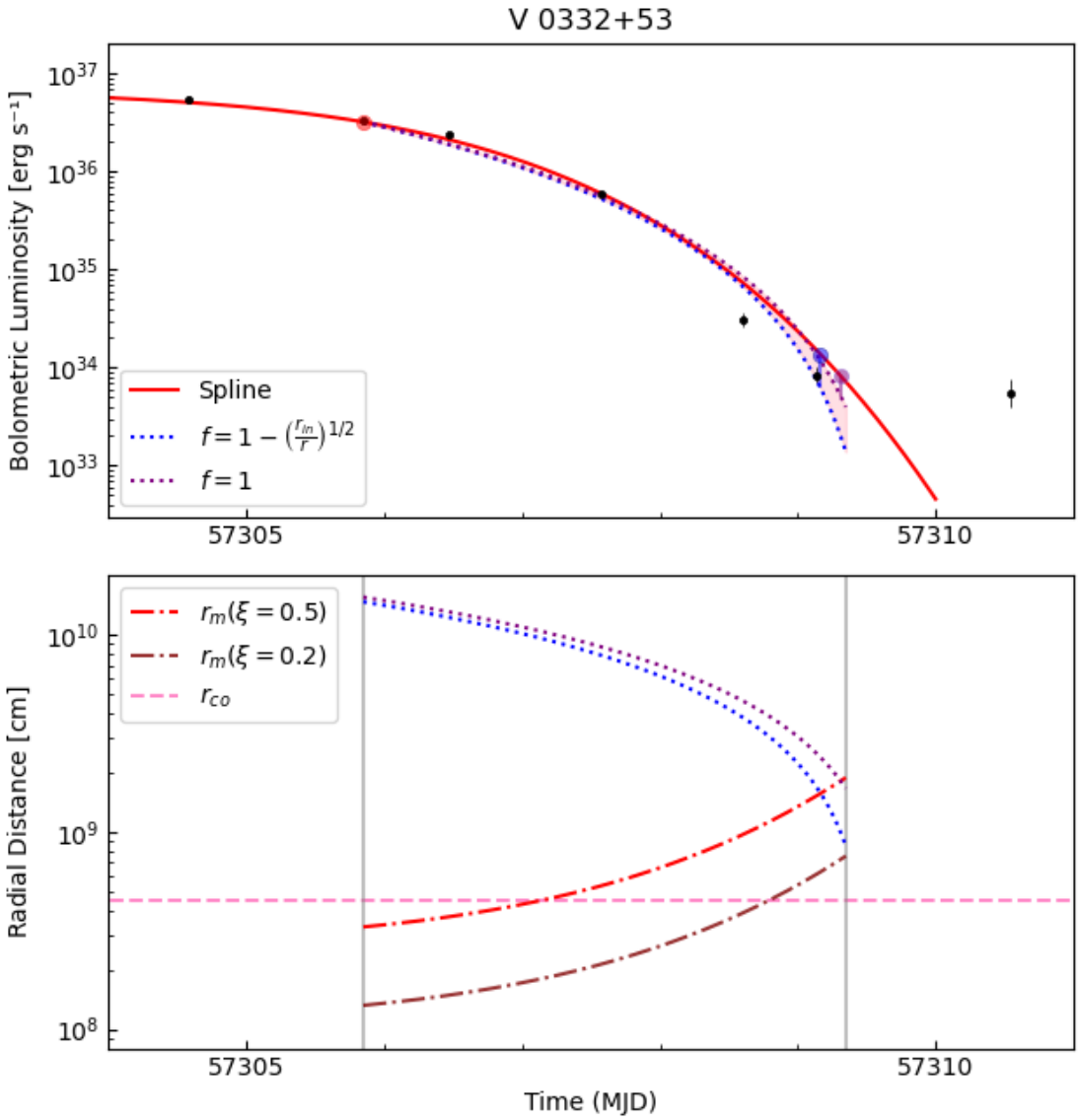

Figure 19. *Top:* The outburst decay of V 0332+53 based on observations made by the *Swift*/XRT telescope. The red line corresponds to the fitted spline, blue and purple corresponds to estimates for the luminosity decay caused by a propagating cooling front. *Bottom:* The evolution of the radial distance of the cooling front compared to the increase in r_m due to decreasing mass accretion rates. The red and brown line corresponds to r_m for $\xi = 0.5$ and $\xi = 0.2$, respectively. The corotation radius r_{co} is shown as a horizontal line (pink).

In addition to finding values of α_{cold}, it is possible to roughly estimate when the cooling front will meet the magnetospheric radius, which corresponds to the inner disk radius r_{in}. It is important to note that the magnetospheric radius r_m is, in fact, also changing during the decay from outburst. By taking into account this fact, the cooling front will "meet" r_m at $\sim 1 \times 10^9$ cm, $\sim 1 \times 10^9$ cm, and $\sim 1.6 \times 10^9$ cm, for SMC X-2, 4U 0115+63, and V 0332+53, respectively. The main takeaways from Figures 17-19 are:

1. The values for α_{cold}, which are adjusted to get a closer fit to the fitted spline, are overall in good agreement with the values for α_{cold} commonly used in the DIM (which assumes $\alpha_{cold} \approx 0.02 - 0.04$).

2. For a rough approximation, the estimated light-curves corresponding to a propagating cooling front, calculated from Equation 24, matches the observed behavior of the sources to reasonable accuracy. This means that one could explain the behavior of the outburst decay by implementing a cooling front.

3. If we also consider whether or not the magnetospheric radius r_m reaches the corotation radius r_{co} before the cooling front reaches r_m, one can see from the bottom part of Figures 17-19 that in all cases, r_m reaches r_{co} before the cooling front "catches up" with r_m. This is in agreement with the division of sources into those entering the propeller regime, and those who avoid it by entering the cold disk regime given in Figure 12, which places SMC X-2, 4U 0115+63, and V 0332+53 into the region of sources entering the propeller regime. It is worth noting that the exact value of r_m is one that is not well known and this means that assuming, e.g., different values of ξ will also ultimately result in different values for L_{prop} (see Equation 15). As seen in the bottom part of Figures 17-19, changing the value of ξ will influence where r_m reaches r_{co}.

5 Summary and conclusions

Highly magnetized accreting X-ray pulsars offer the opportunity to study a plethora of different physical processes responsible for the observational appearances of these objects. The basis of this thesis concerns the relatively unknown behavior of transiently accreting X-ray pulsars at low mass accretion rates. There are currently different mechanisms assumed to be responsible for the observed behavior at low mass accretion rates. Transient X-ray pulsars such as those found in Be/X-ray binaries, provide probes for these mechanisms, thanks to their big range in mass accretion rates, from high values at the peak of their outbursts to low values during the declining phases of the outbursts.

The most common explanation for the declining phases of outbursts into quiescence is the propeller effect. The propeller effect takes place due to exceedingly low mass accretion rates causing an increase in the magnetospheric radius, up to the point of it overtaking the corotation radius. This leads to the formation of a centrifugal barrier which repels matter and halts accretion. Another theory recently put forth is that for certain accreting neutron stars, the centrifugal barrier is sufficiently low for the X-ray pulsar to enter the cold-disk accretion regime, before entering the propeller regime. This concept is commonly invoked to explain the outbursts of dwarf novae, and the theory of their outbursts is encapsulated in the disk-instability model (DIM).

In order to investigate the possibility of using the DIM to explain the light curves of the final stages of outbursts observed in transient X-ray pulsars, the monitoring data collected by *Swift*/XRT on several sources were examined. The light curves of the sample of sources were smoothed by the use of the statsmodels implementation of LOWESS (Locally Weighted Scatterplot Smoothing) and fitted with a spline in order to describe their observed behavior. For the declining phases of the outbursts, predictions made for the luminosity decrease related to the propagation of a cool-

ing front were modeled and compared to the observed behavior represented by the smoothed spline. The obtained values of the α_{cold} parameter, which were adjusted in order to closely match the observations of the outbursts' declining stages, can then be compared to the values predicted by the DIM.

The conclusions made from comparing the observations to the expected behavior of a propagating cooling front, as predicted by a simplified model, is that not only does α_{cold} coincide with the typical values used in the DIM, but the overall appearance of the light curves during the outbursts' declining stages are well described by a cooling front propagating in the accretion disk. Therefore the declining phases of outbursts into quiescence can, in theory, be explained by assuming that the accretion disk is entering the cold state through a propagating cooling front, without the need to necessarily invoke the propeller effect. In order to draw further conclusions about the physical processes responsible for the observational behavior of transient X-ray pulsars, better time resolution is required in order to examine the light-curves of these systems in greater detail as they enter quiescence.

References

[1] R. C. Duncan and C. Thompson. 'Formation of Very Strongly Magnetized Neutron Stars: Implications for Gamma-Ray Bursts'. *Astrophys. J.*, **392**:L9, 1992.

[2] V. L. Ginzburg. 'The Magnetic Fields of Collapsing Masses and the Nature of Superstars'. *Soviet Physics Doklady*, **9**:329, 1964.

[3] L. Woltjer. 'X-Rays and Type I Supernova Remnants'. *Astrophys. J.*, **140**:1309–1313, 1964.

[4] L. D. Landau. 'To the Stars theory'. *Phys. Zs. Sowjet*, **1**:285, 1932.

[5] W. Baade and F. Zwicky. 'Remarks on Super-Novae and Cosmic Rays'. *Physical Review*, **46**(1):76–77, 1934.

[6] A. Hewish *et al.* 'Observation of a Rapidly Pulsating Radio Source'. *Nature*, **217**(5130):709–713, 1968.

[7] L. Bildsten *et al.* 'Observations of Accreting Pulsars'. *Astrophys. J.*, **113**(2):367–408, 1997.

[8] A. P. Igoshev, S. B. Popov, and R. Hollerbach. 'Evolution of Neutron Star Magnetic Fields'. *Universe*, **7**(9):351, 2021.

[9] V. M. Kaspi. 'Grand unification of neutron stars'. *Proceedings of the National Academy of Science*, **107**(16):7147–7152, 2010.

[10] V. M. Kaspi. 'the neutron star zoo'. In *Pulsar Astrophysics the Next Fifty Years*, volume **337**, pages 3–8, 2018.

[11] R. Giacconi *et al.* 'Discovery of Periodic X-Ray Pulsations in Centaurus X-3 from UHURU'. *Astrophys. J.*, **167**:L67, 1971.

[12] E. Schreier *et al.* 'Evidence for the Binary Nature of Centaurus X-3 from UHURU X-Ray Observations.'. *Astrophys. J.*, **172**:L79, 1972.

[13] H. Tananbaum *et al.* 'Discovery of a Periodic Pulsating Binary X-Ray Source in Hercules from UHURU'. *Astrophys. J.*, **174**:L143, 1972.

[14] P. Reig. 'Be/X-ray binaries'. *Astrophys. Space Sci.*, **332**(1):1–29, 2011.

[15] R. Walter and C. Ferrigno. 'X-Ray Pulsars'. In Athem W. Alsabti and Paul Murdin, editors, *Handbook of Supernovae*, page 1385. 2017.

[16] I. Caballero and J. Wilms. 'X-ray pulsars: a review.'. *Mem. Soc. astron. ital.*, **83**:230, 2012.

[17] A. Patruno and A. L. Watts. 'Accreting Millisecond X-ray Pulsars'. *Astrophysics and Space Science Library*, **461**:143–208, 2021.

[18] D. Bhattacharya and E. P. J. van den Heuvel. 'Formation and evolution of binary and millisecond radio pulsars'. *Physics Reports*, **203**(1-2):1–124, 1991.

[19] G. S. Bisnovatyi-Kogan and B. V. Komberg. 'Pulsars and close binary systems'. *Sov. Astron.*, **18**:217, 1974.

[20] M. A. Alpar *et al.* 'A new class of radio pulsars'. *Nature*, **300**(5894):728–730, 1982.

[21] V. Radhakrishnan and G. Srinivasan. 'On the origin of the recently discovered ultra-rapid pulsar'. *Current Science*, **51**:1096–1099, 1982.

[22] P. Kretschmar *et al.* 'Advances in Understanding High-Mass X-ray Binaries with INTEGRAL and Future Directions'. *New Astronomy Reviews*, **86**:101546, 2019.

[23] H. Bondi and F. Hoyle. 'On the mechanism of accretion by stars'. *Monthly Notices Roy. Astron. Soc.*, **104**:273, 1944.

[24] K. Davidson and J. P. Ostriker. 'Neutron-Star Accretion in a Stellar Wind: Model for a Pulsed X-Ray Source'. *Astrophys. J.*, **179**:585–598, 1973.

[25] J. M. Blondin *et al.* 'Enhanced Winds and Tidal Streams in Massive X-Ray Binaries'. *Astrophys. J.*, **371**:684, 1991.

[26] M. Bachetti *et al.* 'An ultraluminous X-ray source powered by an accreting neutron star'. *Nature*, **514**(7521):202–204, 2014.

[27] E. P. J. van den Heuvel and C. De Loore. 'The nature of X-ray binaries III. Evolution of massive close binaries with one collapsed component - with a possible application to Cygnus X-3.'. *Astron. Astrophys.*, **25**:387, 1973.

[28] R. E. Taam and E. L. Sandquist. 'Common Envelope Evolution of Massive Binary Stars'. *Ann. Rev. Astron. Astrophys.*, **38**:113–141, 2000.

[29] J. M. Porter and T. Rivinius. 'Classical Be Stars'. *Publ. Astron. Soc. Pacific*, **115**(812):1153–1170, 2003.

[30] L. A. Balona. 'The Be Phenomenon[1]'. In Myron A. Smith, Huib F. Henrichs, and Juan Fabregat, editors, *IAU Colloq. 175: 'The Be Phenomenon in Early-Type Stars'*, volume **214** of *Astronomical Society of the Pacific Conference Series*, page 1, 2000.

[31] Q. Z. Liu, J. van Paradijs, and E. P. J. van den Heuvel. 'Catalogue of high-mass X-ray binaries in the Galaxy (4th edition)'. *Astron. Astrophys.*, **455**(3):1165–1168, 2006.

[32] M. Revnivtsev and S. Mereghetti. 'Magnetic Fields of Neutron Stars in X-Ray Binaries'. *Space Sci. Rev.*, **191**(1-4):293–314, 2015.

[33] H. Bondi. 'On spherically symmetrical accretion'. *Monthly Notices Roy. Astron. Soc.*, **112**:195, 1952.

[34] Philip J. Armitage. 'Lecture notes on accretion disk physics'. *arXiv e-prints*, 2022.

[35] M. Montesinos. Review: Accretion Disk Theory. *arXiv e-prints*, 2012.

[36] M. A. Abramowicz and O. Straub. Accretion discs. *Scholarpedia*, 9(8):2408, 2014. revision #145813.

[37] S. A. Balbus and J. F. Hawley. 'A Powerful Local Shear Instability in Weakly Magnetized Disks. I. Linear Analysis'. *Astrophys. J.*, **376**:214, 1991.

[38] N. I. Shakura and R. A. Sunyaev. 'Black Holes in Binary Systems: Observational Appearances'. In H. Bradt and Riccardo Giacconi, editors, *X- and Gamma-Ray Astronomy*, volume **55**, page 155, 1973.

[39] J. M. Hameury. 'A review of the disc instability model for dwarf novae, soft X-ray transients and related objects'. *Advances in Space Research*, **66**(5):1004–1024, 2020.

[40] G. Dubus *et al.* 'Testing the disk instability model of cataclysmic variables'. *Astron. Astrophys.*, **617**:A26, 2018.

[41] J. P. Lasota. 'The disc instability model of dwarf novae and low-mass X-ray binary transients'. *New Astronomy Reviews*, **45**(7):449–508, 2001.

[42] S. S. Tsygankov *et al.* 'Stable accretion from a cold disc in highly magnetized neutron stars'. *Astron. Astrophys.*, **608**:A17, 2017.

[43] J. P. Lasota. 'Disc Instabilities and "Soft" X-Ray Transients'. In D. T. Wickramasinghe, G. V. Bicknell, and L. Ferrario, editors, *IAU Colloq. 163: Accretion Phenomena and Related Outflows*, volume **121** of *Astronomical Society of the Pacific Conference Series*, page 351, 1997.

[44] R. F. Elsner and F. K. Lamb. 'Accretion by magnetic neutron stars. I. Magnetospheric structure and stability.'. *Astrophys. J.*, **215**:897–913, 1977.

[45] J. E. Pringle and M. J. Rees. 'Accretion Disc Models for Compact X-Ray Sources'. *Astron. Astrophys.*, **21**:1, 1972.

[46] P. Ghosh and F. K. Lamb. 'Accretion by rotating magnetic neutron stars. III. Accretion torques and period changes in pulsating X-ray sources.'. *Astrophys. J.*, **234**:296–316, 1979.

[47] A. Chashkina *et al.* 'Super-Eddington accretion on to a magnetized neutron star'. *Monthly Notices Roy. Astron. Soc.*, **470**(3):2799–2813, 2017.

[48] F. Khajenabi *et al.* 'Thin accretion disc with a corona in a central magnetic field'. *Astrophys. Space Sci.*, **314**(4):251–260, 2008.

[49] A. F. Illarionov and R. A. Sunyaev. 'Why the Number of Galactic X-ray Stars Is so Small?'. *Astron. Astrophys.*, **39**:185, 1975.

[50] S. S. Tsygankov *et al*. 'Propeller effect in two brightest transient X-ray pulsars: 4U 0115+63 and V 0332+53'. *Astron. Astrophys.*, **593**:A16, 2016.

[51] A. A. Lutovinov *et al*. 'Propeller Effect in the Transient X-Ray Pulsar SMC X-2'. *Astrophys. J.*, **834**(2):209, 2017.

[52] P. Meszaros. *'High-energy radiation from magnetized neutron stars'*. Theoretical Astrophysics, Chicago: University of Chicago Press, 1992.

[53] F. Koliopanos and G. Vasilopoulos. 'Accreting, highly magnetized neutron stars at the Eddington limit: a study of the 2016 outburst of SMC X-3'. *Astron. Astrophys.*, **614**:A23, 2018.

[54] R. Staubert *et al*. 'Cyclotron lines in highly magnetized neutron stars'. *Astron. Astrophys.*, **622**:A61, 2019.

[55] J. K. Daugherty and A. K. Harding. 'Compton Scattering in Strong Magnetic Fields'. *Astrophys. J.*, **309**:362, 1986.

[56] J. Truemper *et al*. 'Evidence for strong cyclotron line emission in the hard X-ray spectrum of Hercules X-1.'. *Astrophys. J.*, **219**:L105–L110, 1978.

[57] M. M. Basko. 'Iron line emission from the Alfven shell in X-ray binaries'. *Astron. Astrophys.*, **87**(3):330–338, 1980.

[58] N. Gehrels *et al*. 'The Swift Gamma-Ray Burst Mission'. *Astrophys. J.*, **611**(2):1005–1020, 2004.

[59] S. D. Barthelmy. 'Burst Alert Telescope (BAT) on the Swift MIDEX mission'. In Kathryn A. Flanagan and Oswald H. Siegmund, editors, *X-Ray and Gamma-Ray Instrumentation for Astronomy XI*, volume **4140** of *Society of Photo-Optical Instrumentation Engineers (SPIE) Conference Series*, pages 50–63, 2000.

[60] S. D. Barthelmy *et al*. 'The Burst Alert Telescope (BAT) on the SWIFT Midex Mission'. *Space Sci. Rev.*, **120**(3-4):143–164, 2005.

[61] D. N. Burrows *et al*. 'The Swift X-Ray Telescope'. *Space Sci. Rev.*, **120**(3-4):165–195, 2005.

[62] P. A. Evans *et al*. 'Methods and results of an automatic analysis of a complete sample of Swift-XRT observations of GRBs'. *Monthly Notices Roy. Astron. Soc.*, **397**(3):1177–1201, 2009.

[63] W. Cash. 'Parameter estimation in astronomy through application of the likelihood ratio.'. *Astrophys. J.*, **228**:939–947, 1979.

[64] H. A. Krimm *et al*. 'the swift/bat hard x-ray transient monitor'. *Astrophys. J. Suppl. Ser*, **209**(1):14, 2013.

[65] J. Tueller *et al*. 'the 22 month swift-bat all-sky hard x-ray survey'. *Astrophys. J. Suppl. Ser*, **186**(2):378–405, 2010.

[66] W. S. Cleveland. 'Robust Locally Weighted Regression and Smoothing Scatterplots'. *Journal of the American Statistical Association*, **74**(368):829–836, 1979.

[67] R. Haschke *et al*. 'Three-dimensional Maps of the Magellanic Clouds using RR Lyrae Stars and Cepheids. II. The Small Magellanic Cloud'. *Astron. J.*, **144**(4):107, 2012.

[68] G. Clark *et al*. 'On two new X-ray sources in the SMC and the high luminosities of the Magellanic X-ray sources.'. *Astrophys. J.*, **221**:L37–L41, 1978.

[69] R. H. D. Corbet *et al*. 'The Discovery of an Outburst and Pulsed X-Ray Flux from SMC X-2 Using the Rossi X-Ray Timing Explorer'. *Astrophys. J.*, **548**(1):L41–L44, 2001.

[70] J. Yokogawa *et al*. 'ASCA Identification of SMC X-2 with the 2.37-s Pulsar Discovered by RXTE'. *Publ. Astron. Soc. Japan*, **53**(2):227–231, 2001.

[71] M. P. E. Schurch *et al*. 'Orbital period determinations for four SMC Be/X-ray binaries'. *Monthly Notices Roy. Astron. Soc.*, **412**(1):391–400, 2011.

[72] L. J. Townsend *et al*. 'On the orbital parameters of Be/X-ray binaries in the Small Magellanic Cloud'. *Monthly Notices Roy. Astron. Soc.*, **416**(2):1556–1565, 2011.

[73] N. La Palombara *et al*. 'Spectral analysis of SMC X-2 during its 2015 outburst'. *Monthly Notices Roy. Astron. Soc.*, **458**(1):L74–L78, 2016.

[74] G. K. Jaisawal and S. Naik. 'Detection of cyclotron resonance scattering feature in high-mass X-ray binary pulsar SMC X-2'. *Monthly Notices Roy. Astron. Soc.*, **461**(1):L97–L101, 2016.

[75] R. Giacconi *et al*. 'The Uhuru catalog of X-ray sources.'. *Astrophys. J.*, **178**:281–308, 1972.

[76] W. Forman *et al*. 'The fourth Uhuru catalog of X-ray sources.'. *Astrophys. J. Suppl. Ser*, **38**:357–412, 1978.

[77] L. Cominsky *et al*. 'Discovery of 3.6-s X-ray pulsations from 4U0115+63'. *Nature*, **273**(5661):367–369, 1978.

[78] S. Rappaport *et al*. 'Orbital elements of 4U 0115+63 and the nature of the hard X-ray transients.'. *Astrophys. J.*, **224**:L1–L4, 1978.

[79] M. Johns *et al.* '4U 0115+63'. *IAU Circ.*, **3171**:1, 1978.

[80] I. Negueruela and A. T. Okazaki. 'The Be/X-ray transient 4U 0115+63/V635 Cassiopeiae. I. A consistent model'. *Astron. Astrophys.*, **369**:108–116, 2001.

[81] L. Whitlock *et al.* 'Observations of the X-Ray Transient 4U 0115+63'. *Astrophys. J.*, **338**:381, 1989.

[82] W. A. Wheaton *et al.* 'An absorption feature in the spectrum of the pulsed hard X-ray flux from 4U0115 + 63'. *Nature*, **282**(5736):240–243, 1979.

[83] N. E. White *et al.* 'Accretion powered X-ray pulsars.'. *Astrophys. J.*, **270**:711–734, 1983.

[84] W. A. Heindl *et al.* 'Discovery of a Third Harmonic Cyclotron Resonance Scattering Feature in the X-Ray Spectrum of 4U 0115+63'. *Astrophys. J.*, **521**(1):L49–L53, 1999.

[85] A. Santangelo *et al.* 'A BEPPOSAX Study of the Pulsating Transient X0115+63: The First X-Ray Spectrum with Four Cyclotron Harmonic Features'. *Astrophys. J.*, **523**(1):L85–L88, 1999.

[86] W. A. Heindl *et al.* 'Timing and Spectroscopy of Accreting X-ray Pulsars: the State of Cyclotron Line Studies'. In Philip Kaaret, Frederick K. Lamb, and Jean H. Swank, editors, *X-ray Timing 2003: Rossi and Beyond*, volume **714** of *American Institute of Physics Conference Series*, pages 323–330, 2004.

[87] J. Terrell *et al.* 'X-ray transients as seen by Vela, 1969-1979'. In W. Brinkmann and J. Truemper, editors, *Accreting Neutron Stars*, pages 210–212, 1982.

[88] L. Stella *et al.* 'The discovery of 4.4 second X-ray pulsations from the rapidly variable X-ray transient V 0332+53.'. *Astrophys. J.*, **288**:L45–L49, 1985.

[89] I. Negueruela *et al.* 'The Be/X-ray transient V0332+53: evidence for a tilt between the orbit and the equatorial plane?'. *Monthly Notices Roy. Astron. Soc.*, **307**(3):695–702, 1999.

[90] K. Makishima *et al.* 'Discovery of a Prominent Cyclotron Absorption Feature from the Transient X-Ray Pulsar X0331+53'. *Astrophys. J.*, **365**:L59, 1990.

[91] M. T. Stollberg *et al.* 'GRO J1008-57'. *IAU Circ.*, **5836**:1, 1993.

[92] M. J. Coe *et al.* 'Now you see it, now you don't - the circumstellar disc in the GRO J1008-57 system'. *Monthly Notices Roy. Astron. Soc.*, **378**(4):1427–1433, 2007.

[93] M. S. Riquelme *et al.* 'Circumstellar emission in Be/X-ray binaries of the Magellanic Clouds and the Milky Way'. *Astron. Astrophys.*, **539**:A114, 2012.

[94] A. M. Levine and R. Corbet. 'Detection of Additional Periodicities in RXTE ASM Light Curves'. *The Astronomer's Telegram*, **940**:1, 2006.

[95] T. Yamamoto *et al*. 'Discovery of cyclotron-line feature at 76 keV from Be/X-ray binary pulsar, GRO J1008-57'. *The Astronomer's Telegram*, **4759**:1, 2013.

[96] C. R. Shrader *et al*. 'High-Energy Spectral and Temporal Characteristics of GRO J1008-57'. *Astrophys. J.*, **512**(2):920–928, 1999.

[97] F. Meyer. 'Limit cycle instabilities in accretion disks'. In W. Brinkmann and J. Truemper, editors, *Accreting Neutron Stars*, pages 333–337, 1982.

[98] F. Meyer. 'Transition waves in accretion disks'. *Astron. Astrophys.*, **131**(2):303–308, 1984.

[99] J. Frank *et al*. *'Accretion power in astrophysics.'*, volume **21**. Camb. Astrophys. Ser., 1992.